Nuclear Engineering and Design 241 (2011) 4026–4044

Contents lists available at ScienceDirect

Nuclear Engineering and Design

journal homepage: www.elsevier.com/locate/nucengdes

PARIS project: Radiolytic oxidation of molecular iodine in containment during a nuclear reactor severe accident: Part 2. Formation and destruction of iodine oxides compounds under irradiation – Experimental results modelling

L. Bosland[a,*], F. Funke[b], G. Langrock[b], N. Girault[a]

[a] Institut de Radioprotection et de Sûreté Nucléaire, DPAM, SEMIC, LETR – BP 3, 13115 Saint Paul lez Durance, France
[b] AREVA NP GmbH, Radiochemical Laboratory, P.O. Box 1109, D-91001 Erlangen, Germany

ARTICLE INFO

Article history:
Received 16 August 2010
Received in revised form 6 June 2011
Accepted 7 June 2011

ABSTRACT

In the case of a severe accident in a nuclear Light Water Reactor (LWR), the high radiation fields reached in the reactor containment building due to the release of fission products from the reactor core would induce air radiolysis. The air radiolysis products (ARP) could, in turn, oxidise gaseous molecular iodine (I_2) into aerosol-borne iodine–oxygen–nitrogen compounds, abbreviated as iodine oxides (IO_x). These reactions involve the conversion of a gaseous iodine compound resulting in a change of the iodine depletion rate from the containment atmosphere. Kinetic data were produced within the first part of PARIS project on the air radiolysis products formation and destruction. The second part of the PARIS project as presented in this paper deals with the impact of the ARP on the conversion of I_2 into IO_x. The objective was to provide a database to develop new or to validate existing kinetic models of formation and destruction of iodine oxides.

The iodine tests of the PARIS project, performed at very low, realistic iodine concentrations, constitute an important database to further develop or validate empirical and mechanistic models on radiolytic I_2 oxidation. In the presence of painted surface areas or silver aerosol surface areas, radiolytic I_2 oxidation is negligible compared to I_2 adsorption on these surfaces for the conditions examined. However, radiolytic I_2 oxidation remains very efficient if surface areas are small or if they are made of the relatively non-reactive stainless steel.

1. Introduction

In the case of a severe accident in a nuclear Light Water Reactor (LWR), a large amount of radioactive fission products (FP) may be released from the reactor core into the reactor containment, leading to a high dose rate at short term that rapidly decreases down to about 1 kGy h^{-1} inside the containment. Those dose rates are typical of the long term phase of an accident and persistent on the long-scale of weeks/months. Thus, this represents a potential important radiological hazard to the environment. Iodine is considered to be one of the major radiotoxic elements. Knowledge of iodine behaviour in such conditions is therefore necessary to evaluate the possible release in the environment and study the impact of iodine mitigation measures to prevent or minimize iodine release to the environment. PHEBUS tests were performed to study the fuel and control rods degradation processes, FP transport and behaviour in the containment involved in such an accident (Clement et al., 2003; Girault et al., 2006, 2009; Gregoire et al., 2008; Hanniet and Repetto, 1999; Jacquemain et al., 2000, 1997; Schwarz et al., 1999; Simondi-Teisseire, 2008; Payot et al., 2010). Iodine behaviour was particularly investigated in these tests. The iodine inventory in the containment atmosphere depends on numerous physico-chemical processes such as deposition at and resuspension from surfaces, reactions in sumps and in containment atmosphere, and iodine exchange between sump and atmosphere. Furthermore, iodine speciation and thus iodine volatility is influenced by these processes.

An important chemical process in the high irradiative atmosphere, caused by the radionuclides released to the containment, is the radiolytic oxidation of molecular iodine (I_2) into iodine oxides (IO_x) (Funke et al., 1999; Vikis and MacFarlane, 1985). As a consequence, a volatile gaseous iodine species is converted into an aerosol-borne iodine species, which means that the gas-borne iodine depletion rate by deposition could be changed. Previous experiments revealed that the destruction of molecular iodine (I_2) can be explained as a reaction of I_2 with air radiolysis products (ARP) (Funke et al., 1999) such as ozone (O_3), nitrogen dioxide (NO_2), nitric acid (HNO_3) and many other short-lived products

* Corresponding author.
E-mail address: loic.bosland@irsn.fr (L. Bosland).

0029-5493/$ – see front matter © 2011 Elsevier B.V. All rights reserved.
doi:10.1016/j.nucengdes.2011.06.015

(radicals such as HO•, O•, e⁻ . . .) (Bosland et al., 2008). ARP are formed by the radiolysis of the air/steam containment atmosphere and can be destroyed in a high radiation field. An empirical model on radiolytic oxidation of I_2 into IO_x including formation and destruction of ARP and including earlier Canadian work (Vikis and MacFarlane, 1985) on the reaction between I_2 and ozone was derived under the conditions of high initial I_2 concentrations as compared to severe accident conditions (Funke et al., 1999). The resulting model predicts a very fast conversion of I_2 into IO_x, and that iodine gaseous phase speciation is dominated by iodine oxides rather than by I_2.

Quantifying IO_x size and composition in representative irradiation conditions is a very challenging work that has never been done. However, as mentioned earlier, ozone is one of the main oxidising ARP that can react with I_2. THAI tests investigated the reaction of I_2 with O_3 (used as a simulant of oxidising ARP that would be normally produced under irradiation) (Sonnenkalb and Poss, 2009; Funke et al., submitted for publication). It was found that the formation of IO_x in particle form is very efficient, e.g. at an O_3 excess over I_2 of more than two orders of magnitude, complete conversion of gaseous I_2 into particulate IO_x took place within less than 3.4 h, and volume-related diameters of particles were up to about 0.35 μm. However, the underlying database was built only at comparably high I_2 and/or O_3 concentrations, and the influence of surfaces as present in LWR containments on the competition between iodine deposition and radiolytic I_2 oxidation into IO_x was not considered in these experiments.

Consequently, implementation of this empirical model on radiolytic oxidation into severe accident iodine codes would have been premature. The development of mechanistic models on radiolytic iodine oxidation (Aubert, 2002; Dickinson and Sims, 2000; Narayanan, 2000) also suffers from a lack of experimental data.

The Program on Air Radiolysis and Iodine adsorption on Surfaces (PARIS) was therefore initiated in 2002 by IRSN (Institut de Radioprotection et de Sûreté Nucléaire) and performed in collaboration with AREVA NP (formerly Framatome ANP) with the objective of measuring:

- the rate and amount of air radiolysis products (ARP) production and destruction,
- rate and extent of radiolytic oxidation of molecular iodine into iodine oxides,
- the effect of the containment structural surfaces, namely decontamination coating ("paint") and stainless steel, on radiolytic oxidation of I_2,
- the effect of silver, representing silver-containing aerosol particles, on radiolytic oxidation of I_2.

Important features of the PARIS project as compared to the previous work were (1) low iodine concentrations, (2) surface to volume ratios of paint, steel and silver surface areas representative of LWR and/or PHEBUS-FP containments, (3) steam fractions and (4) dose rates representative of LWR or PHEBUS-FP containments.

The PARIS database was intended to provide data to develop and validate empirical models, and finally to derive a simplified model for severe accident source term evaluation such as ASTEC (Accident Source Term Evaluation Code) (Allelein et al., 2005, 2003, 2008; Bosland et al., 2010a; Cousin et al., 2008; van Dorsselaere, 2008; van Dorsselaere et al., 2010, 2005, 2009; Weber et al., 2009) and other severe accident iodine codes.

The PARIS database includes about 400 tests, about half of them including iodine. The tests whose objective was to measure the kinetics of ARP formation and destruction in the presence of surfaces were presented in a previous paper together with the interpretation of their results (Bosland et al., 2008). Concentrations of ARP up to 1×10^{-6} mol L^{-1} were measured depending on dose rate, temperature and chemical composition of the gaseous phase. The test series involving iodine are presented and interpreted in the current paper.

2. Experimental

The objectives of these experiments were to determine the kinetics of formation of iodine oxides from gaseous molecular iodine and to quantify the effect of different surfaces (stainless steel AISI 316L, RIPOLIN paints and metallic silver) on iodine oxides formation within boundary conditions (atmospheric composition, temperature, dose rate, areas of surfaces) representative to LWR containments and PHEBUS facility containments.

The general experimental procedure was to establish the desired composition of gases in 1-l glass flasks with the option of adding surface coupons, to irradiate the glass flasks at given dose rates representative of the long-term dose rates during an accident until the desired doses were reached, and to subsequently determine the gaseous iodine species and iodine oxides amount formed by an off-line method.

2.1. Irradiations

Irradiations were performed at the Co-60 source of the Technische Universität München at Garching at the same conditions described in our previous paper (Bosland et al., 2008). Typically, dose rates of 0.3 and 1 kGy h^{-1} were applied at temperatures of 80 °C or 130 °C to study the long term gaseous iodine chemistry in the containment.

Doses between 0.05 kGy and 100 kGy were achieved. Due to the finite dimensions of the glass flasks, the dose rate might had differed to some extent at different points within the flask, with respect to the measured dose rate in the centre. However, this difference is considered to be negligible in the frame of the overall uncertainties associated with the irradiated test results.

Heating was performed by immersion into heating baths. The temperature of the bath was kept constant throughout the irradiation with a heating plate regulated to provide a constant temperature with a variation of less than ±5 K. After the irradiation, any coupons were recovered prior to the analyses of the air radiolysis products.

2.2. Filling of the flasks

For cleaning, the glass flasks (Duran® borosilicate glass) were washed with acetone and water and heated up to 500 °C at least for 6 h in order to remove all potential organic impurities.

The total volume of the glass flasks is 1.12×10^{-3} m^3, and the inner surface area is 6.8×10^{-2} m^2. Thus, the surface area/volume ratio is 60.7 m^{-1}.

The experimental apparatus for filling the flasks is shown in Fig. 1. The glass flasks were heated up to the desired temperature of the subsequent irradiation and evacuated. The filling procedure consisted of: (1) evacuating the glass flasks, (2, if needed) pressure-controlled addition of H_2 (4%, v/v hydrogen) to the flask and then (3) bubbling of air (or O_2) through the I_2 dosing flask in the water bath until ambient pressure was reached. The flasks were in the hot-air cabinet which was heated to the temperatures of the tests.

Pressure equilibration with the ambient pressure was then obtained by introducing mixtures of air/30%, v/v steam or oxygen/30%, v/v steam mixtures. Synthetic air (<0.1 ppm hydrocarbon (C_nH_m, NO_x) and <0.5 ppm H_2O) or oxygen (purity >99.999%; <0.2 ppm hydrocarbon (C_nH_m), <3 ppm H_2O and <0.2 ppm C_nH_m and CO_2) were provided by "Linde" or "Air Liquide". When investigating the effect of surface samples, these were introduced in the "batch" reactor before evacuating and filling with gases.

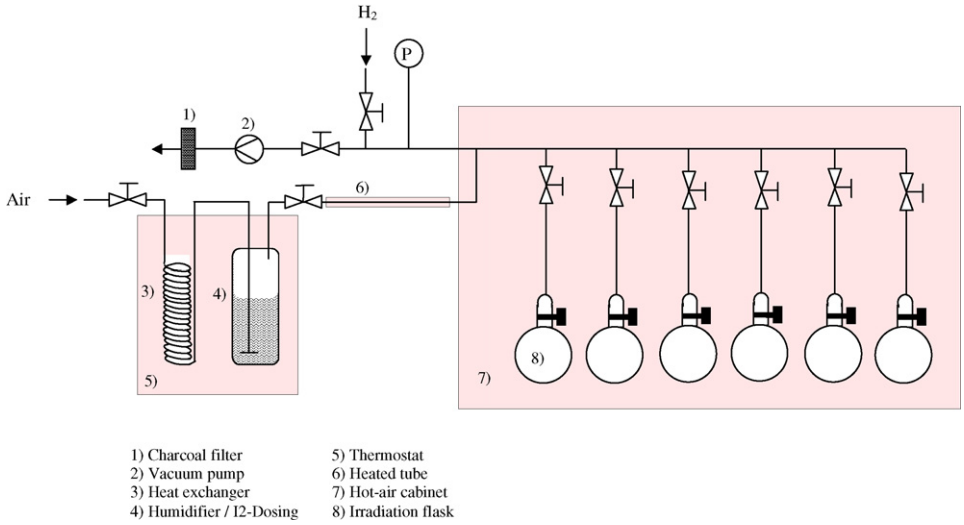

Fig. 1. Filling of glass flasks before irradiation in PARIS tests. Up to 6 glass flasks are filled in one step.

The air/steam or oxygen/steam mixtures were obtained by passing air or oxygen through a thermostated water bath (Milli-Q quality). The pure gases were passed through a humidifier at a defined temperature to obtain gas mixtures containing the demanded steam content. This humidifier contained also iodine (in the tri-iodide I_3^- form) in order to transfer gaseous I_2 from the liquid phase to the gaseous phase. The gaseous I_2 concentration was controlled by the temperature in the humidifier and the aqueous iodine concentration (solution of I_2/I_3^- traced with ^{123}I at a pH around 6).

The humidifier and the glass flasks were connected through a heated tube, mainly with Teflon surface. Heating was provided to minimize unwanted deposition of I_2 and to prevent condensation of steam. Inside the hot air cabinet, most parts of the line were made of glass to minimize unwanted I_2 deposition. Up to 6 glass flasks could be filled in one batch. It turned out during the first irradiation campaigns that only the filling of 3 flasks made sense, as the temperature losses between end of filling and installing in the heating baths near the irradiation source could lead to unwanted condensation of steam. In the presence of iodine, I_2 (^{123}I) could then be hydrolysed even before the irradiation has started. This had to be avoided. In addition, batch-wise filling enabled the filling of flasks with different contents (e.g. three flasks with synthetic air, and another three flasks with synthetic air + hydrogen).

Control measurements of initial I_2 concentrations (indicated as $[I_2]^\circ$ in this paper) in the flasks were performed by analysing one of the filled flasks directly after filling, as explained in the next section. Iodine was washed from this control flask and determined directly. Establishing detailed desired initial iodine concentration was difficult to control, e.g. due to losses in the transport lines, ageing of the I_2/I_3^- solution (mainly by hydrolysis) and control of other parameters of the filling facility.

2.3. Experimental determination of gaseous I_2 concentration in the flasks

2.3.1. Post-test liquid–liquid extraction

Firstly, the liquid–liquid extraction procedure was developed in order to discriminate gaseous I_2 from iodine oxides formed during irradiation. It was assumed that IO_x species comprise all species of oxidised iodine, irrespective of the detailed stoichiometry and including IN_yO_x compounds. However, the stability of IN_yO_x compounds is currently investigated by theoretical means as only one publication is available in the literature Filistovic and Nedveckaite (1999), which suggests that they are not stable above 0 °C.

After removing the surface samples from the flask, tetrachloromethane (CCl_4) was injected into the flask. After cooling down to room temperature, water was injected and the flask was shaken to wash out all iodine species from the gaseous phase and from the inner glass surfaces. The resulting two liquid phases were transferred to a separatory funnel and separated. The result of this step is the separation of the sum of oxidised iodine (assumed to be in the iodate form (IO_3^-) once dissolved) and I^- on one hand from the I_2/organic iodine fraction on the other hand. One can question this procedure as I_2 is also soluble in water and decomposes into HOI and I^-. Then, HOI decomposes into IO_3^- so that aqueous I_2 could lead to overestimate IO_x amount. However, these two reactions are pH dependant. Under our extraction conditions (pH = 7) the following statement can be made:

- According to the Lin work (Lin, 1980), HOI is "suspected" to be accounted for in the aqueous fraction, not in the organic phase. In liquid–liquid-extractions with only I_2, a small amount of activity in the aqueous phase could thus not only be an artefact due to limited quality of phase separation, but also due to HOI.
- Thus, some HOI is suspected to be formed but iodates formation is only fast enough in a basic pH regime (Bell et al., 1982), i.e. at least the iodates are of no concern to us.

Moreover, we verified with non-irradiated tests (e.g. no iodine oxides are formed) that I_2 is mainly found in the organic CCl_4 phase (> 90%).

Consequently, the uncertainties of I_2 and IO_x concentrations are clearly dominated by

- Insufficient phase separation during the liquid–liquid extraction procedure (estimated at about 5%) (small amount of I_2 can also be transferred into the liquid phase).
- The CCl_4 droplets remaining stuck on the glass walls after having separated both phases but not by gamma counting (5% maximum).

An overall uncertainty on the measurement of 10% maximum is thus relevant (the uncertainty on gamma counting is negligible compared to those ones).

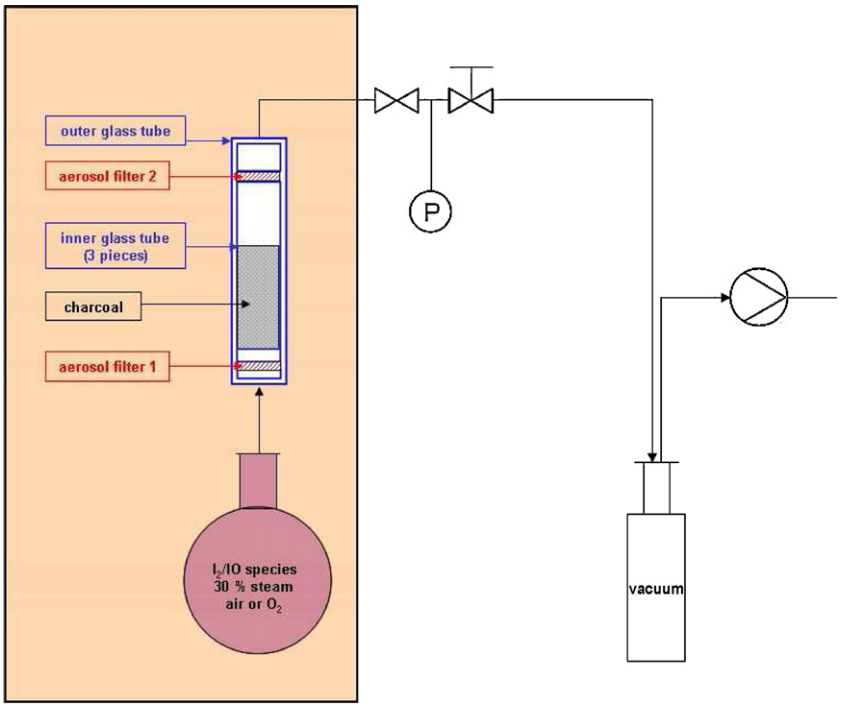

Fig. 2. PARIS Maypack to discriminate IO_x particles (aerosol filter cartridge 1) and gaseous iodine (I_2, RI, charcoal filter cartridge).

2.3.2. Separation with a filter unit (PARIS Maypack)

Another separation method with the objective to discriminate between the gas-borne iodine species "iodine aerosols" and "volatile iodine" was also developed in the course of the PARIS project. It was based upon the idea that volatile iodine is non-reacted I2 or organic iodide (if painted steel coupons were present during the irradiation), and that the reacted iodine (oxidised iodine) is in the aerosol form. It is noted that the well-known iodine oxides I_2O_5 and I_4O_9 are only stable in the solid state. There is, however, no information about the stable states of other iodine oxides so their behaviour on the PARIS Maypack is not known a priori. To some extent the PARIS Maypack can also serve to check the results of the liquid–liquid extraction procedure. It was expected that the PARIS Maypack would provide more accurate separation results for I_2 and IO_x quantification than the liquid–liquid extraction procedure. However, the Maypack does not account for the iodine species deposited onto the glass surface. The latter is safely assessed only by the liquid–liquid extraction.

The PARIS Maypack consists of two glass tubes shown in Fig. 2. The inner glass tube is divided into three parts. Between the lower and the middle unit, a quartz filter is fixed as an aerosol catcher. The charcoal as I_2/RI absorber is separated from the quartz filter by a holey glass plate circa 1 cm above the quartz filter. This arrangement avoids the contamination of the quartz filter by charcoal particles. The second quartz filter closes the filter unit. The outer glass tube acts as a stabilizer. The whole unit was placed together with the glass flask to be evacuated by a vacuum pump in a hot-air cabinet and is operated there. The material of the quartz filter was supplied by Schleicher and Schüll, filtering aerosols larger than 0.3 μm. As THAI tests showed particles of about this size, the efficiency of the quartz filter could be questioned. However, we are confident in its efficiency for the following reasons:

- Tests were performed in the same boundary conditions but with post-test analyses using either the liquid–liquid extraction method and/or the Maypack method. The remaining I_2 concentrations were found to be the same, usually within about 10% of the total amount of iodine in each test. We concluded that the aerosol filter of the Maypack was efficient enough to retain at least the large majority of particulate, gas-borne IO_x.
- Gas-borne IO_x was only found as a minority. Measurements showed that most of the IO_x particles are deposited onto the glass surface and are not transferred to the Maypack. Even if they were extremely small, this can be due to a fast agglomeration of these particles under the given experimental conditions, or due to the fact, that post-test analyses with Maypack filtering and liquid–liquid extraction was performed a significant time after irradiation has stopped. In this time, agglomeration could have taken place and enlarge particles which are then trapped on filters with much higher efficiency.

A contamination of the first quartz filter with I_2 or RI could only occur if it was wet, but the experimental procedure prevented condensation. Contamination of the quartz filter by charcoal can also be excluded due to the spatial separation of charcoal from the filter with a glass plate with pin holes. Charcoal was used with an amount that safely can remove RI and I_2 from the gas stream through the filter unit. But there is another limitation: it is not known of what size the formed aerosol particles were. It could happen that the quartz filter did not separate particles of a certain size. One can assume that those aerosols would then deposit to a certain extent evenly in the charcoal. On the other hand, the aerosols let through the quartz filters would have been only a small cut-out of a typical aerosol size distribution. From there, an uncertainty can be estimated as follows: the possible loss of activity on the quartz filter is assumed to be 5%. The activity in the charcoal may then be over-determined to 5% of the activity on the first quartz filter. The second quartz filter has mainly to prevent powdered charcoal to the vacuum pump and to remove any residual aerosols from the gas stream. Since its measured activities are always very low, an estimation of the uncertainty was not performed. However, the design of the PARIS Maypack significantly reduces possible experimental errors in iodine speciation in the determination of the most important species significantly.

Table 1
Geometric dimensions of the different coupons of PARIS tests. V is the gaseous volume (m^3) of the used glass flasks, S is the coupon surface area (m^2). LWR means approximate values for a typical LWR containment.

Substrate	Stainless steel	Epoxy paint	Silver
Length (cm) × width (cm) × height (cm)	0.8 × 0.8 × 0.5	1.3 × 1.0 × 0.5	14.9 × 0.75 × 0.025
Surface area (cm^2)	2.88	4.9	23.1
Objective S/V (cm^{-1}) LWR/PHEBUS FP	3×10^{-3}	5×10^{-3}	2×10^{-2} (LWR)
PARIS: ratio surface coupon/glass surface	4.2×10^{-3}	7.2×10^{-3}	3.4×10^{-2}

2.4. Surface samples characteristics and analysis

The surface types and surface areas studied in the PARIS program (stainless steel, epoxy paint and silver) had to be chosen to be representative of LWR and PHEBUS facility containments

- Stainless steel is the main component of the primary circuit (Schwarz et al., 1999). Other structural components are providing stainless steel surfaces such as ladders, cable trays, PHEBUS vessel walls were made of AISI 316L steel (Jacquemain et al., 2000). In support to PHEBUS tests interpretation, the same type of steel was chosen.
- Epoxy paints surfaces were chosen as they cover the containment surfaces that account for tens of thousands square meters can be painted with Epoxy paint in a LWR. In PHEBUS, they were scaled to investigate iodine behaviour under realistic conditions (Schwarz et al., 2001). The same S/V ratio was kept for PARIS tests.
- Silver is one of the elements of the control rods that is known to be highly reactive towards iodine. Indium and cadmium, two others element used in PWR control rods, are not known to interact strongly with iodine. As large amount of this silver could be transported towards the containment in case of accident, the interaction of iodine with airborne silver is necessary.

The geometric characteristics of the used surface samples are given in Table 1.

The chemical composition of stainless steel coupons (AISI 316L) is indicated in Table 2. They contain 2 wt% Mo which should provide greater protection against pitting and thus also should weaken their corrosion by halogens, and in particular, iodine.

The coating of the epoxy paint coupons contains a mixture of a polymer (an alcohol polyamine) and a hardener (consisting of an epoxy liquid from a bisphenol (60%) plus a cycloaliphatic polyamine (30%)). Pigments (such as SiO_2 and TiO_2) are also contained in the coating of the paint.

Silver was provided by Johnson Matthey (purity > 99.9%) in the form of foils. Before experiments, the silver surface was washed with water and acetone and then heated for cleaning. It had a shiny appearance, thus guaranteeing the absence of any important oxide layer on the surface stemming e.g. from storage at ambient conditions.

Coupons were placed at the bottom of the flasks. According to their geometrical forms they provided deposition surface areas that consist of both, vertical and horizontal surfaces. This has to be taken into account for modelling of aerosol settling and gaseous iodine adsorption. After the end of the test, the I-123 activity on the surface of the coupons was determined by gamma spectrometry. The uncertainty associated to this counting was estimated to be 10% for steel and painted coupon. For silver coupons, it was estimated at 30%, mainly due to the errors of the determined geometry factors. Analyses of iodine speciation on the surface coupons were not performed due to the extremely low concentrations.

All results and data available from these tests are summarized in Table 5 (gaseous tests only, no surfaces introduced) and Table 7 (when surfaces were introduced in the glass vessel).

3. Models description

In the first part of this work, i.e. with tests in the absence of iodine, a mechanistic code (IRSN-IODAIR) was shown to be suitable for predicting air radiolysis products formation (Aubert, 2002). In the presence of iodine, the modelling of the data with the numerous chemical reactions involving air radiolysis products and iodine radiolytic products was not fully satisfying. However, we intend in the future from PARIS program and its interpretation to develop a fundamental understanding of the reaction between iodine and ARP that will lead to complete the mechanistic models able to reproduce iodine behaviour.

A phenomenological model gave a reasonable description of air radiolysis products formation (Funke et al., 1999; Bosland et al., 2008) and this is extended in this paper by a phenomenological reaction between iodine and air radiolysis products to analyse the experimental PARIS data including iodine. The use of the phenomenological model is also favoured by two additional advantages: (1) it is consistent, as required for the present PARIS tests including iodine, with commonly used phenomenological iodine deposition and desorption models and organic iodine release models, and (2) its simplicity saves computing time, as compared to mechanistic models if included in containment codes such as ASTEC (Bosland et al., 2010a; van Dorsselaere et al., 2009) and COCOSYS (Allelein et al., 2008). The phenomenological models that will be used to analyse PARIS iodine tests are described in this section.

Fig. 3 summarizes the main phenomena considered relevant for the interaction of iodine and steel (left) and epoxy paint (right). The models considered in this work are described in the following sections with their associated kinetics.

3.1. Air radiolysis products formation and destruction

The phenomenological model relative to ARP production in the absence of iodine was developed in the first part of this project (Bosland et al., 2008):

$$\frac{d[\mathrm{ARP}]}{dt} = k_1 \cdot D - k_3 \cdot [\mathrm{ARP}] \cdot \mathrm{D} - k_D \cdot \frac{S}{V} \cdot [\mathrm{ARP}] \quad \text{(I)}$$

with [ARP]: gaseous air radiolysis products concentration ($mol\,m^{-3}$); k_1: ARP formation rate constant ($mol\,m^{-3}\,Gy^{-1}$); k_3: ARP destruction rate constant (Gy^{-1}); k_D: ARP destruction rate constant due to ARP destruction at a surface ($m\,s^{-1}$); D: dose rate in the gaseous phase ($Gy\,s^{-1}$); S: surface area of the surface coupon introduced in the vessel (m^2); and V: volume of the vessel (m^3).

Table 2
Chemical composition of the 316L stainless steel coupons.

Element	Ni	Cr	Fe	C	Mn	S	Si	P	Co	Mo
Weight fraction (%)	10.5–13	16–18	Bal.	<0.03	<2	0.03	0.75–1	0.04	0.2	2–2.4

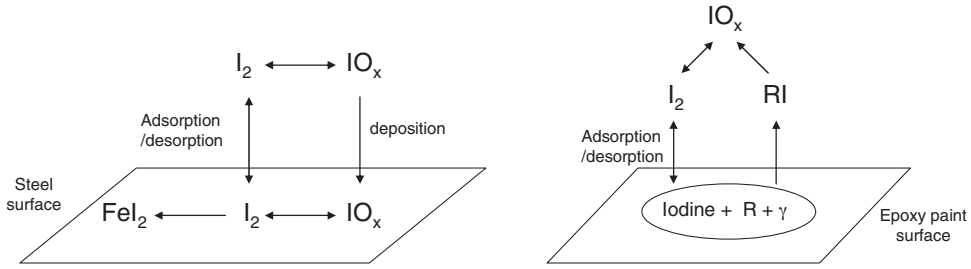

Fig. 3. Illustration of phenomena considered relevant for the interaction of iodine with steel (left) and with epoxy paint (right). (Not all processes are included in the modelling of this work, see Section 3. Not shown is the conceivable conversion of iodine adsorbed on the paint by gaseous ARP into IO_x analogously to the process on steel.)

Table 3
Rate constants of ARP formation and destruction in an air/steam mixture at 80 °C from part I of this publication and their associated activation energies (E_a).

	k_1 (10^{11}) ($mol\,L^{-1}\,Gy^{-1}$)	k_3 (10^4) (Gy^{-1})
	8.64	3.6
E_a ($kJ\,mol^{-1}$)	0	31.2

Default values of the rate constants are given in Table 3. This empirical model treats the ARP production as a zero-order process whereas ARP destruction is described by a first-order kinetics law. As surfaces usually lead to the depletion of ARP concentration, this model also includes a destruction term due to the presence of these surfaces even if the PARIS tests in the absence of iodine (Vikis and MacFarlane, 1985) did not reveal a conclusive effect of epoxy paint or of stainless steel 316L on the ARP concentrations.

3.2. Iodine oxides formation and destruction

Iodine oxides are formed in the phenomenological concept by the reaction of ARP with molecular iodine (I_2). The formation of iodine oxides (IO_x) is described by a second order model originally developed by Vikis and MacFarlane (1985). This model had been extended by Funke et al. (1999) to also reproduce the non-negligible remaining I_2 fractions even at large doses, by adding a reaction path from IO_x back to I_2 simulating a reverse reaction to the radiolytic I_2 oxidation:

$$\frac{1}{2}\cdot\frac{d[IO_x]}{dt} = -\frac{d[I_2]}{dt} = k_2\cdot[ARP]\cdot[I_2] - \frac{1}{2}\cdot k_6\cdot D\cdot[IO_x] \quad \text{(II)}$$

with $[I_2]$: gaseous I_2 concentration ($mol\,m^{-3}$); k_2: iodine oxides formation rate constant ($m^3\,mol^{-1}\,s^{-1}$); k_6: iodine oxides destruction rate constant (Gy^{-1}); D: dose rate in the gaseous phase ($Gy\,s^{-1}$); and $[IO_x]$: concentration of iodine oxides ($mol\,m^{-3}$).

Default values of the rate constants are given in Table 4.

This model assumes immediate particle growth. The expression IO_x in this model implicates a number of physico-chemical aspects:

- The stoichiometric index "x" remains undefined as oxygen is not modelled or balanced in the phenomenological model.
- The process of nucleation, i.e. the pathway from the primarily formed IO_x molecules in the (thermochemically instable) gaseous state into solid state (IO_x in aerosol form) is not considered explicitly. The evaluation of the PARIS data using this model implicates the transformation of I_2 in a gaseous state directly into IO_x in an aerosol form. This is also a prerequisite for selecting gas/particle discrimination filters to distinguish between I_2 and IO_x in the present PARIS tests.

Table 4
Rate constants of IO_x formation from previous analyses by Vikis and MacFarlane (1985) and Funke et al. (1999).

Temperature (°C)	k_2 (10^{11}) ($L\,mol^{-1}\,s^{-1}$)	
	Funke	Vikis
20	100…10,000	2250
80	300…30,000	9900
130	500…15,000	15,000

The introduction of the IO_x formation to the air radiolysis model entrains an additional ARP depletion term to Eq. (I) that is illustrated by Eq. (Ia):

$$\frac{d[ARP]}{dt} = -k_2\cdot R\cdot[ARP]\cdot[I_2] \quad \text{(Ia)}$$

with $R = 3.9$ (Funke et al., 1999; Vikis and MacFarlane, 1985).

3.3. Organic iodides formation and destruction

I_2 deposition onto the painted coupon surface is an alternative pathway to radiolytic I_2 oxidation in the PARIS tests including painted coupons. This I_2 may efficiently react within the paint to form organic iodides at or within the painted surface. Driven by radiolytic reactions and according to their volatility at enhanced temperatures, organic iodides can be released from such paints. A corresponding phenomenological model is used in this work (Funke, 1999) using the chemical formula for methyl iodide (CH_3I) to designate the whole class of released volatile organic iodides. The destruction of volatile organic iodides was modelled by Tang and Castelman (1970) and this model was confirmed later (Dickinson et al., 2003). Both kinetics are summarized in Eq. (III).

$$\frac{d[CH_3I]}{dt} = k_{RI}\cdot D\cdot[Iodine]_{paint}^{0.43}\cdot\frac{S}{V} - k_{dt}\cdot D\cdot[CH_3I] \quad \text{(III)}$$

with $[CH_3I]$: gaseous concentration of CH_3I ($mol\,m^{-3}$); $[Iodine]_{paint}$: total iodine loading on paint ($mol\,m^{-2}$); k_{RI}: rate constant of CH_3I release from iodine-loaded paint ($1.87\times10^{-9}\,mol^{0.57}\,m^{-1.15}\,Gy^{-1}$ at 25 °C); D: dose rate in the gaseous phase ($Gy\,s^{-1}$); S: painted coupon area (m^2); V: gaseous volume (m^2); and k_{dt}: radiolytic destruction rate of organic iodides (Gy^{-1}) in the gaseous phase.

The model does not distinguish between different iodine species on the paint (physisorbed or chemisorbed). To produce organic iodides after I_2 deposition, a reaction with organic molecules of the paint needs of course to take place, and this process is implicitly included in the model.

A thermal production of RI is also possible (Funke, 1999). However, it can be neglected in front of the production due to irradiation.

3.4. I_2 adsorption and desorption from surfaces

I_2 is known to be adsorbed and desorbed from steel, paints and silver surfaces. The phenomenological model is described in the

following Eq. (IV) and implies that one I_2 molecule produces two adsorbed iodine atoms:

$$\frac{d[I_2]}{dt} = k_{ads} \cdot [I_2] \cdot \frac{S}{V} - k_{des} \cdot \frac{[\text{Iodine}]_{surface}}{2} \cdot \frac{S}{V} \quad \text{(IV)}$$

with k_{ads}: adsorption constant of I_2 onto the coupon ($m\,s^{-1}$); k_{des}: desorption constant of I_2 from surface (s^{-1}); and $[\text{Iodine}]_{surface}$: iodine concentration onto the surface ($mol\,m^{-2}$).

In PARIS test modelling, S is the surface area of the painted coupon or of the stainless steel coupon.

This simplified physisorption model ignores that I_2 reacts chemically with paint and steel surfaces, but it is used due to its simplicity to describe a side reaction besides the radiolytic I_2 oxidation. Rate constants will be given later in this paper when the model is compared to the experiments.

3.5. Iodine oxides settling and deposition onto surfaces

The modelling performed in this work (Sections 4 and 5) does not include deposition of IO_x onto the coupons, i.e. neither the adsorption of gaseous IO_x nor the settling of IO_x in particle form because of a lack of data (e.g. deposition velocities and particle size distribution) of these compounds. From the horizontal arrangement of the coupons, both processes could have taken place during the tests. Even if possible at the extremely low iodine concentrations on the coupon surface, a determination of iodine species at the surface would not provide an unambiguous result. In fact, this iodine speciation could also have been changed during the test, e.g. by conversion of deposited I_2 into deposited IO_x, as just one example of a number of possible secondary processes that were not considered during PARIS tests.

4. Iodine oxides formation and destruction in the absence of surface coupons

4.1. Experimental results

The extent of radiolytic I_2 oxidation in the absence of containment-relevant surfaces was studied during the PARIS program by measuring the amounts of produced iodine oxides and remaining I_2. Discrimination of these two iodine species was mainly based upon liquid–liquid extraction (I_2 in the organic fraction, IO_x in the aqueous fraction) followed by ^{123}I tracer measurement. Additionally, results from tests with I_2/IO_x discrimination based upon their different physical states (gaseous/particulate) on a simplified Maypack filter are included. The graphs built from the experimental data are mostly histograms displaying the remaining iodine fraction (I_2) on the left scale and the iodine products fraction (IO_x) versus the absorbed dose. Essentially two different dose ranges were investigated (about 1 and 15 kGy). The figures also display through a straight line the initial I_2 concentration in the glass flask, referring to the right scale. Applying the chosen I_2 injection into the glass flasks to establish extremely low initial I_2 concentrations means that it was very difficult to control and obtain the same initial I_2 concentrations in repeated loadings.

Various conditions were investigated. The composition of the gaseous phase was varied in order to highlight the influences of oxygen, nitrogen and hydrogen at a fixed steam concentration of 30% in the vessel. Temperature influence was also studied, by performing irradiations at 80 °C and 130 °C.

In the following sections, the relative iodine amounts (%) recovered after the tests are displayed in the figures. These experimental data have to be read with the left ordinate scale whereas the initial I_2 concentration has to be read on the right ordinate scale.

4.1.1. Influence of the gaseous phase composition

Fig. 4 displays the relative amounts of iodine oxides and I_2 for different absorbed doses and initial I_2 concentrations at 80 °C. It can be concluded that, for initial I_2 concentrations lower than about 10^{-7} mol L^{-1}, I_2 conversion into IO_x is only partial for doses of about 1 kGy. For doses of around 15 kGy, I_2 conversion is almost complete. Moreover, the higher the absorbed dose the higher is the conversion of I_2 into IO_x. If the initial I_2 concentration is increased up to around 10^{-6} mol L^{-1}, the percentage of conversion of I_2 into IO_x seems to decrease.

The results provided in Fig. 4 demonstrate an appreciable scattering of the conversion results in comparable test conditions. This holds for example for the sets of tests performed at around 1.1 kGy, at around 15 kGy, and at around 18 kGy. Given the large scattering of ARP formation already observed in Bosland et al. (2008) and also in analogous older tests of ARP formation from other studies cited in Bosland et al. (2008), the scattering of the conversion yields of I_2 by ARP in this paper is not surprising. An additional contribution to the scattering of data in the tests with iodine in this paper is given by the limited accuracy of the iodine species separations, especially if a small fraction of iodine species is to be measured in presence of

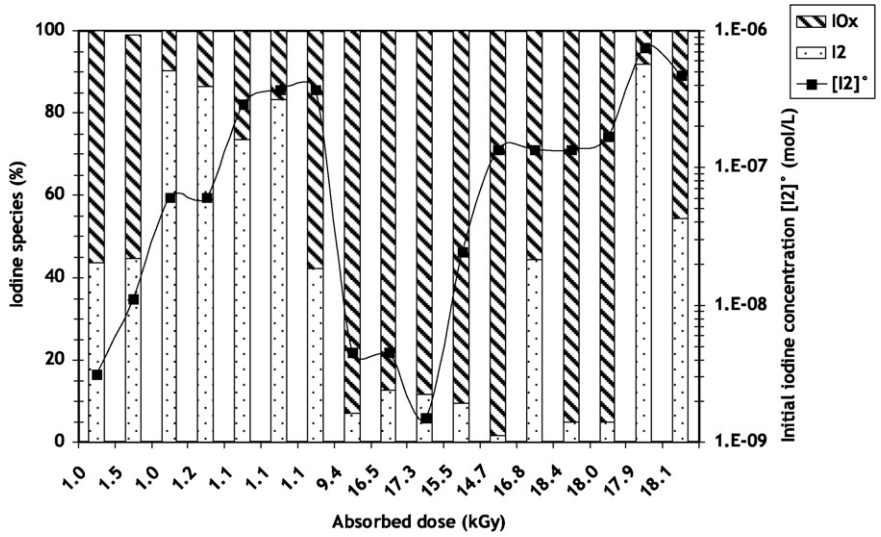

Fig. 4. Relative amount of iodine oxides and I_2 in irradiated air/steam 30% (v/v) mixture at 80 °C as a function of absorbed doses and initial gaseous I_2 concentration (dose rate close to 1 kGy h^{-1}).

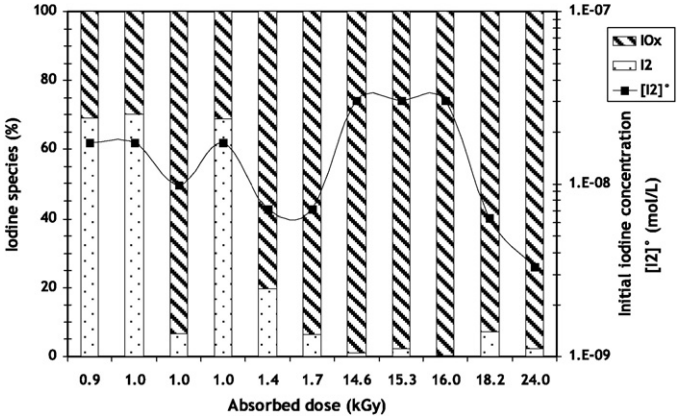

Fig. 5. Relative amount of iodine oxides and I_2 in irradiated O_2/steam (30%) mixtures at 80 °C as a function of absorbed doses and initial gaseous I_2 concentration (dose rate close to 1 kGy h^{-1}).

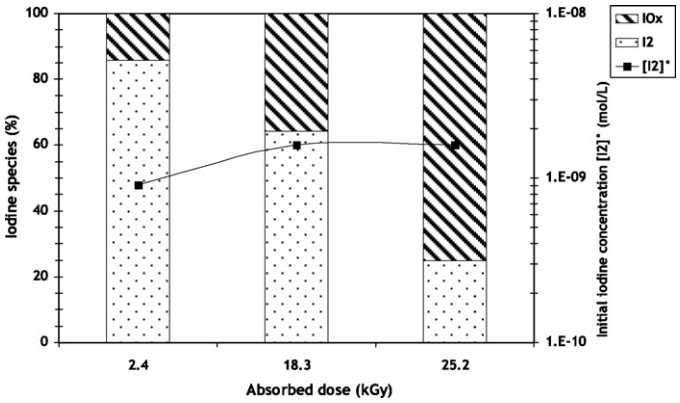

Fig. 7. Relative amount of iodine oxides and I_2 in irradiated air/steam (30%) mixtures at 130 °C as a function of absorbed doses and initial gaseous I_2 concentration (dose rate close to 1 kGy h^{-1}).

a huge excess of (the) other iodine species. These same problems of scattered conversion yields and the reasons for their scattering also hold for the data presented in the following sections.

Fig. 5 shows iodine oxide yields in an O_2/steam atmosphere at 80 °C, i.e. results on IO_x formation in the absence of nitrogen. For initial iodine concentrations lower than about 10^{-8} mol L^{-1}, the conversion into iodine oxides is almost complete even for low absorbed doses. For higher initial iodine concentrations, the conversion is complete for doses close to 15 kGy or higher, but not at 1 kGy. As no data are available for intermediate doses between 1 and 15 kGy, the detailed evolution of the conversion into IO_x with dose is not measured. From comparison with Fig. 4 it is deduced that IO_x formation is more efficient in O_2/steam atmospheres than in air/steam atmospheres. Replacing nitrogen from air/steam atmospheres by oxygen using O_2/steam atmospheres obviously increases the oxidation potential. One explanation is that the amount of the oxidant $O^\bullet$ radical formed in that case is more important than in a nitrogen/steam atmosphere.

Fig. 6 provides IO_x formation yields at 80 °C in air/steam atmospheres in conditions comparable to those of Fig. 4, but here the test atmospheres additionally contain 4% hydrogen. The conversion of molecular iodine is significantly smaller when hydrogen is present. The presence of reducing radiolysis products ($H^\bullet$...) is proposed to slow down the I_2 oxidation, as these can react with the oxidising products from the air/steam radiolysis ($HO^\bullet$, $O^\bullet$...), thereby depleting the oxidising products required for I_2 oxidation.

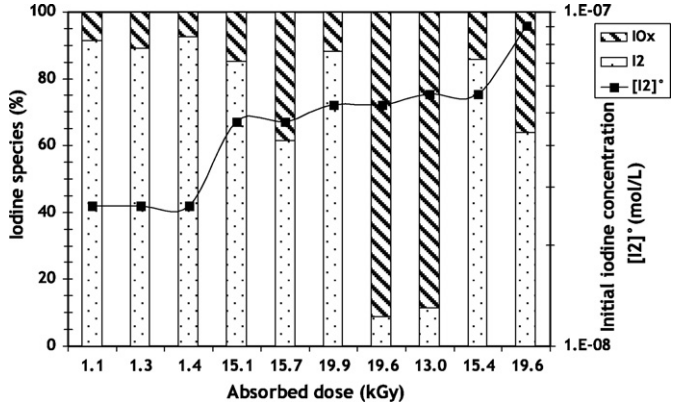

Fig. 6. Relative amount of iodine oxides and I_2 in irradiated air/steam (30%)/H_2 (4%) mixtures at 80 °C as a function of absorbed doses and initial gaseous I_2 concentration (dose rate close to 1 kGy h^{-1}).

4.1.2. Influence of the temperature

The influence of temperature was studied by performing some tests at 130 °C, to be compared with the major fraction of tests done at 80 °C. However, no clear trends could be observed from Fig. 7 because of the small amount of data, in combination with its scattered nature, as discussed above. The few results available seem to show that the fraction of iodine oxides formed at 130 °C is lower than at 80 °C. Another tendency is that the higher the absorbed dose, the higher is the I_2 conversion for similar initial I_2 concentrations, which is consistent with the effect at 80 °C.

The small decrease in the fraction of IO_x with increasing temperature could be linked either to a decrease of I_2 radiolytic oxidation rate and/or to an increasing iodine oxides decomposition rate.

4.1.3. Influence of NO_2 and N_2O on iodine oxides formation

I_2 oxidation by nitrogen dioxide (NO_2) and nitrous oxide (N_2O) was investigated in non-irradiated tests at 80 °C in air/30% steam atmospheres. It had been evidenced that the N–O compounds are major ARP during irradiation for high absorbed doses (Bosland et al., 2008). The objective was therefore to study the direct impact of these two N–O species on IO_x formation, i.e. formation of IO_x in less complex test conditions as compared to the irradiated tests. As discussed in the introduction, the term IO_x also includes all compounds in the I–N–O system. From direct injection, NO_2 concentrations were at 5.1×10^{-6} mol L^{-1} and N_2O concentrations at 7.4×10^{-7} mol L^{-1} and at 6.8×10^{-6} mol L^{-1}. Initial I_2 concentrations were between 1.5×10^{-9} mol L^{-1} and 6.2×10^{-9} mol L^{-1}, i.e. lower than NO_x concentrations by least 2 orders of magnitude. Even after exposure times of up to 18.5 h at 80 °C, no clear evidence of IO_x formation was observed. This could be linked with the low thermal stability of $IONO_2$, supposed to be one of the first compounds precursor to the nitroxides aerosols nucleation (Filistovic and Nedveckaite, 1999), or implicate a radical mechanism for formation of iodine nitrogen oxide species that would be very slow.

4.2. Modelling of the data

The phenomenological model presented by Eqs. (III) and (IV) were implemented in the FACSIMILE Software that is able to solve differential equations applied to chemistry field (FACSIMILE, 2008). Rate constants for ARP formation and destruction were taken from the previous article (Bosland et al., 2008) and are summarized in Table 3.

Table 4 summarizes available rate constants for IO_x formation (k_2) from the literature Funke et al. (1999) and Vikis and MacFarlane (1985). The k_2 values from Vikis and MacFarlane (1985) were used during the present modelling work, as they were

determined with higher accuracy, and as the corresponding rate constants from Funke et al. (1999) are consistent with those from Bosland et al. (2008). For the decomposition rate of IO_x, a value of $k_6 = 3.6 \times 10^{-6}\,Gy^{-1}$ is used in this study, which is in the range of k_6 values suggested in Funke et al. (1999). However, a more precise determination of k_6 would be needed, and this is part of the current EPICUR project (Guilbert et al., 2008, 2007). This reaction is important for the whole phenomenological model, as it limits the IO_x formation to finite amounts rather than completing I_2 conversion into IO_x.

As essentially only 2 dose ranges were studied – at around 1 kGy and at around 15 kGy – detailed evolutions of IO_x yields with dose are not available from the PARIS tests. However, effects of atmosphere or initial I_2 concentration were elaborated experimentally, and all these effects could finally lead to a refinement of the described kinetic model.

The model proposed in this document does not explicitly take into account different atmospheric compositions, as they were experimentally tested to highlight a potential influence of oxygen and hydrogen on IO_x formation. The tested atmosphere composed of air/30% steam is relevant for accidents in a reactor containment, and emphasis is laid on the modelling of the data from those tests with the air/steam atmospheres.

Fig. 8 shows the evolutions of molecular iodine and iodine oxide fractions at 80 °C calculated with the phenomenological model for an initial I_2 concentration of $1.37 \times 10^{-7}\,mol\,L^{-1}$ in an air/30% steam atmosphere. Also included are data for which test conditions are suitable enough to compare experimental I_2 and IO_x fractions with the model. The model predicts a nearly total conversion of I_2 at doses higher than 10 kGy. The three comparable experiments are in relatively good agreement with the model, if the above discussed data scattering and their discussed origins is reflected. As there are no data at lower doses, the calculated low-dose evolution of I_2 and IO_x fractions before reaching nearly complete I_2 conversion into IO_x cannot be assessed.

Fig. 9 provides a comparison of data and model in air/30% steam at 80 °C with variation of the initial I_2 concentration, i.e. the experimental data are the same as in Fig. 4. In Fig. 9 the relative deviations of modelled and experimental I_2 and IO_x fractions are displayed (the reference is the experimental data). For low doses, the agreement between the data and the modelling is rather satisfying, irrespective of the initial iodine concentration. At high doses the comparison shows higher discrepancies in some tests for I_2 prediction, which could be due to the above-discussed data scattering. Measuring very low amounts of I_2 by the liquid–liquid extraction is uncertain and challenging as a small fraction of IO_x can be solubilised into the organic phase. This could lead to an overestimation of the remaining I_2 amount. Another explanation could be the limited accuracy of the model for the low initial I_2 concentrations. In fact, the majority of iodine was converted into IO_x and this is quite well reproduced by the model. However, the model remains uncertain for predicting very low remaining I_2 amounts at initial I_2 concentrations lower than $1 \times 10^{-7}\,mol\,L^{-1}$, meaning that the experimental data are underestimated by a factor ranging from 10 to 1000. Above $1 \times 10^{-7}\,mol\,L^{-1}$ and high doses, the agreement between the model and data is better again.

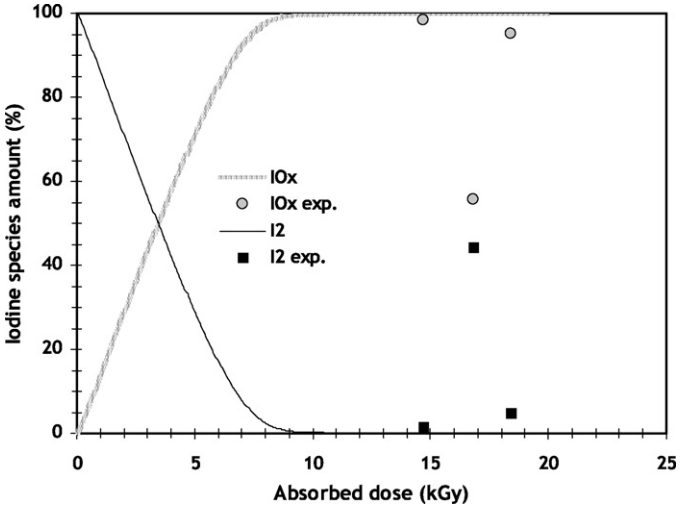

Fig. 8. Evolution of the relative amount of iodine oxides and I_2 at 80 °C as a function of absorbed doses ($[I_2]^\circ = 1.37 \times 10^{-7}\,mol\,L^{-1}$ and dose rate close to $1\,kGy\,h^{-1}$) and comparison with the experimental data for an air/steam 30% mixture.

5. Iodine oxides formation and destruction in the presence of surface coupons

A second step in the present work was to study the effect of surfaces on the extent of radiolytic I_2 conversion into IO_x. In such systems, deposition of I_2 onto the surfaces competes with

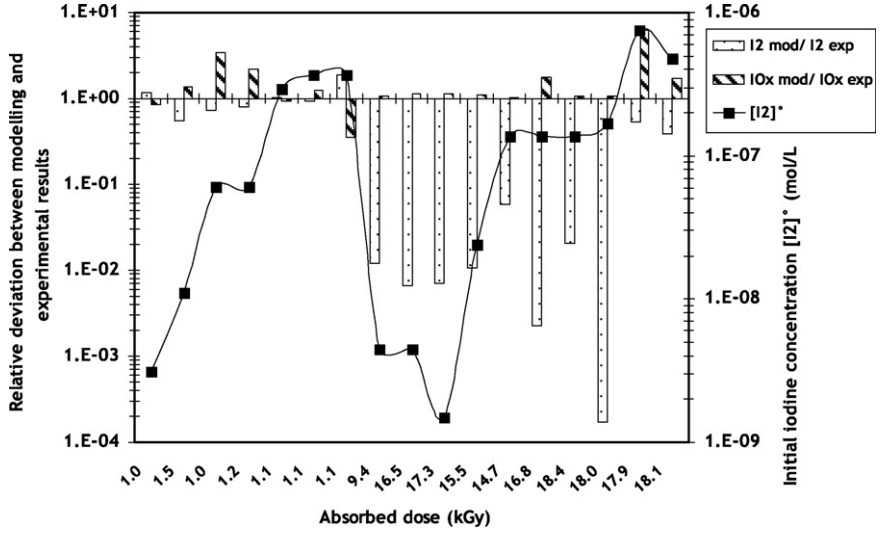

Fig. 9. Relative deviation* between modelling and experimental data (irradiated air/steam 30% (v/v) mixture) for iodine oxides and I_2 modelled at 80 °C as a function of absorbed doses and initial gaseous I_2 concentration (dose rate close to $1\,kGy\,h^{-1}$). *The baseline at 1.E+00 on the ordinate scale refers to experimental data.

Table 5
Summary of experimental data on radiolytic conversion of molecular iodine into iodine oxides (IO_x) in the absence of surfaces.

Test conditions	Test name	$[I_2]^\circ$ (mol L^{-1})	Dose (kGy)	Gaseous I_2 (%)	IO_x (%)
Air 30% steam 80 °C	6V21	3.1E−09	1.0	43.6	56.4
	8V2	1.1E−08	1.5	44.6	54.4
	4V24	6.1E−08	1.0	90.2	9.8
	4V25	6.1E−08	1.2	86.5	13.5
	7V3	2.9E−07	1.1	73.5	26.5
	7V11	3.7E−07	1.1	83.3	16.7
	7V12	3.7E−07	1.1	42.1	57.9
	11T12	4.5E−09	9.4	7.1	92.9
	11T23	4.5E−09	16.5	12.7	87.3
	8V9	1.5E−09	17.3	11.6	88.4
	6V18	2.4E−08	15.5	9.5	90.5
	5V4	1.4E−07	14.7	1.7	98.3
	5V5	1.4E−07	16.8	44.2	55.8
	5V6	1.4E−07	18.4	4.8	95.2
	7V10	1.7E−07	18.0	4.9	95.1
	3V6	7.5E−07	17.9	91.9	8.1
	3V10	4.8E−07	18.1	54.3	45.7
Air 30% steam 4% H_2 80 °C	4V14	2.6E−08	1.1	91.4	8.6
	4V15	2.6E−08	1.3	89.2	10.8
	4V13	2.6E−08	1.4	92.6	7.4
	4V16	4.7E−08	15.1	85.3	14.7
	4V20	4.7E−08	15.7	61.6	38.4
	5V7	5.3E−08	19.9	88.2	11.8
	5V8	5.3E−08	19.6	8.9	91.2
	4V9	5.7E−08	13.0	11.5	88.5
	4V10	5.7E−08	15.4	85.8	14.2
	5V19	9.1E−08	19.6	63.9	36.1
O_2 30% steam 80 °C	3V19	1.7E−08	0.9	69.0	31.0
	3V18	1.7E−08	1.0	70.1	29.9
	6V26	9.8E−09	1.0	6.6	93.4
	6V17	7.2E−09	1.4	19.8	80.2
	6V16	7.2E−09	1.7	6.5	93.5
	3V14	3.0E−08	14.6	1.1	98.9
	3V13	3.0E−08	15.3	2.3	97.8
	3V15	3.0E−08	15.9	0.3	99.7
	6V31	6.3E−09	18.2	7.2	92.8
	9V21	3.3E−09	24.0	2.4	97.6

radiolytic I_2 oxidation, and this competition may depend on the type and structure of the surface. Three different surface types were therefore tested for the reasons explained below:

- Stainless steel, electro-polished, as an important surface area in PHEBUS-FP tests (Gregoire et al., 2008; Hanniet and Repetto, 1999; Jacquemain et al., 2000; Payot et al., 2010) that needs to be studied to better understand I_2 interaction with steel.
- Painted surfaces, made of epoxy paint onto a steel substrate, as an important surface areas in nuclear reactor containments and in PHEBUS-FP tests. Ripolin type was chosen as representative of the paint used in French nuclear power plants.
- Silver, to simulate silver aerosols which could act as effective I_2 sinks due to the formation of non-volatile silver iodide. As it was not possible to perform irradiated tests with suspended aerosols, silver was used in the PARIS tests as a metal foil, which at least covers the pure chemical effect. Silver aerosols would not be pure in the containment in case of accident but mixed with other elements coming from the core of the reactor (Kissane, 2008) as observed in PHEBUS FPT1 test (Jacquemain et al., 2000). However, these other elements are not reactive towards iodine as silver is. Clearly, these tests do not provide silver surface areas per unit mass that are representative for reactor accident containments, but this specific surface area is already contained in silver/iodine models and can be used for evaluating the effect of Ag/I_2 interaction in the present irradiated tests.

In the case of steel and paint, the ratios of surface area/volume were always chosen to be representative of LWR or PHEBUS-FP containments, as shown in Table 1.

5.1. Tests without irradiation

Before studying the effect of irradiation, some tests were performed in non irradiating conditions to evaluate the kinetics of adsorption molecular iodine on these surfaces.

Exposure times were 20 min, 40 min or 60 min in an air – 30% steam atmosphere at 80 and 130 °C and the results are summarized in Table 6. A small amount of iodine was always detected in the liquid phase of the liquid–liquid extraction and formally assigned to the iodine oxide fractions. However, no iodine oxides should be formed in the non-irradiated conditions. As mentioned in Section 2.3.1 discrimination of iodine species with the liquid–liquid extraction method is only accurate down to a level of a few percent since these few percent fractions could have erroneously been distributed into the respective wrong liquid phase. As a consequence, the sum of iodine detected in both liquid phases is considered to be volatile, non-adsorbed I_2. This interpretation is reflected in the two following figures (Figs. 10 and 11) displaying the effect of I_2 adsorption onto the different surface types at 80 °C and at 130 °C, respectively.

For steel surfaces, low adsorption is for the investigated initial iodine concentrations (around 0.5×10^{-7} and 3×10^{-7} mol $\times$ L^{-1}). The majority of the initial iodine inventory remained in the I_2 gaseous form. No clear evolution is detected after the first sampling at 20 min despite the different iodine initial concentrations investigated at 20 min and 40 min. A rapid equilibrium of I_2 distribution between the gas phase and surface could have been reached in the vessel, but this conclusion remains uncertain as only few data are available. At 130 °C and for lower concentration of iodine, a similar fraction is adsorbed onto the steel surface Fig. 11 and no evolution with time could be highlighted.

Table 6
Summary of experimental data on conversion of molecular iodine into iodine oxides (IO_x) in the presence of surfaces (no irradiation).

Test conditions	Surface type	Test name	$[I_2]^\circ$ (mol L^{-1})	Exposure time	Gaseous I_2 (%) (or RI + I_2)	IO_x (%)[a]	I_2 adsorbed onto surface (%)
80 °C – air steam (30%)	Steel (3 cm^2)	5V12	2.0E−07	20	88.8%	8.2%	2.9%
		5V1	2.5E−08	40	93.0%	2.8%	4.2%
		5V9	2.9E−07	60	84.9%	10.5%	4.6%
	Ag (22 cm^2)	5V13	2.0E−07	20	14.6%	2.6%	82.8%
		5V2	2.5E−08	40	53.7%	1.2%	45.2%
		6V13	5.2E−08	40	22.1%	3.3%	74.7%
		5V10	2.9E−07	60	5.0%	3.3%	91.7%
	Paint (4 cm^2)	5V14	2.0E−07	20	66.5%	6.0%	27.4%
		6V10	5.2E−08	20	61.9%	11.4%	26.7%
		5V3	2.5E−08	40	76.7%	3.0%	20.3%
		6V11	5.2E−08	40	65.0%	6.9%	28.1%
		5V11	2.9E−07	60	11.4%	7.0%	81.6%
		6V12	5.2E−08	60	54.7%	8.0%	37.3%
130 °C – air steam (30%)	Steel (3 cm^2)	8V38	1.2E−09	20	32.2%	63.3%	4.6%
		8V39	1.2E−09	40	61.4%	23.7%	14.9%
		8V40	1.2E−09	60	49.1%	43.5%	7.4%
		10V6	5.8E−09	20	72.0%	22.5%	5.4%
		10V7	5.8E−09	40	69.2%	21.1%	9.7%
		10V8	5.8E−09	60	73.3%	19.8%	6.9%
	Ag (22 cm^2)	8V41	1.0E−09	20	0.0%	0.0%	100.0%
		8V42	1.0E−09	40	0.3%	11.9%	87.8%
		8V43	1.0E−09	60	0.8%	0.0%	99.2%
		9V7	1.5E−09	20	2.5%	0.9%	96.5%
		9V8	1.5E−09	40	1.9%	5.9%	92.2%
		9V9	1.5E−09	60	1.5%	6.5%	92.0%
	Paint (4 cm^2)	9V10	1.4E−09	20	68.3%	9.4%	22.3%
		9V11	1.4E−09	40	56.3%	15.1%	28.6%
		9V12	1.4E−09	60	47.7%	9.7%	42.6%

[a] The small amount of iodine oxides is most probably be due to limitations of the liquid–liquid extraction procedure and was considered as I_2 in the analyses of the results.

For silver and paint, a similar iodine behaviour is noted at 80 °C and 130 °C in Figs. 10 and 11: iodine adsorption increases with time between 0 and 60 min, except for silver at 130 °C for which almost all iodine was adsorbed onto the surface after 20 min. Moreover, iodine adsorption on silver is stronger than on paint. No influence of the temperature or the initial iodine concentration can be noted.

5.2. Stainless steel surface

5.2.1. Experimental results

Fig. 12 shows the speciation at the end of the irradiation when a steel coupon was introduced into the vessel as a function of dose and initial iodine concentration. It can be concluded that very little iodine was adsorbed onto the coupon during the irradiation tests, except for two tests for which adsorbed iodine is the main species (at 1.67 and 16.49 kGy). For doses of about 1 kGy, the results are very close to those obtained without surfaces, i.e. I_2 and IO_x were found in similar fractions.

At the high dose range, the conversion of I_2 into IO_x is almost complete for initial iodine concentrations lower than 1×10^{-7} mol L^{-1}. The influence of the initial I_2 concentration onto the conversion into IO_x is not obvious. The test for which adsorbed iodine had been the main species (16.5 kGy in Fig. 12) is considered as outlier: increased I_2 deposition onto the steel surface due

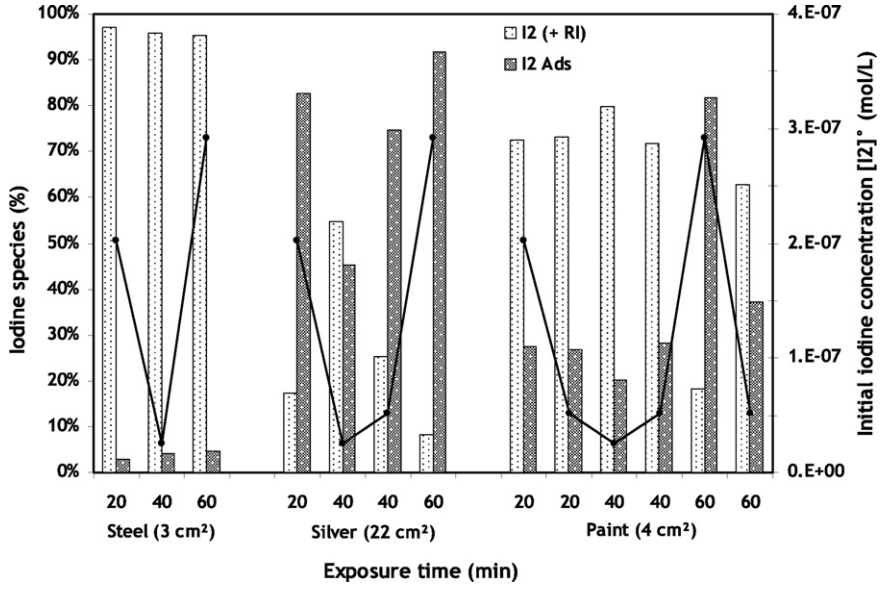

Fig. 10. Relative speciation (histograms, left axis) of iodine species at 80 °C in air/steam 30% mixture when surfaces are introduced in the glass vessel as a function of time and initial I_2 concentration (full black lines, right axis) (no irradiation; no iodine oxides are considered to be formed in these experiments).

Table 7
Summary of experimental data on radiolytic conversion of molecular iodine into iodine oxides (IO_x) in the presence of surfaces.

Test conditions	Surface type	Test name	$[I_2]^\circ$ (mol L^{-1})	Dose (kGy)	Gaseous I_2 (%) (or RI + I_2)	IO_x (%)	Adsorbed I_2 onto surface (%)
Air 30% steam 80 °C	Steel (3 cm^2)	6V22	3.1E−09	1.4	34.1	55.2	10.7
		8V4	5.7E−09	1.7	50.5	34.2	15.3
		4V22	5.1E−08	1.0	61.7	30.6	7.7
		6V4	5.5E−08	1.3	57.2	39.2	3.7
		9V24	3.0E−09	16.9	6.4	84.8	8.9
		6V19	2.4E−08	20.9	0.7	97.1	2.1
		6V7	3.3E−08	16.0	0.6	98.6	0.8
		3V9	4.8E−07	16.5	11.0	10.0	79.1
		6V2	5.5E−08	48.5	0.2	98.2	1.6
Air 30% steam 80 °C	Paint (5 cm^2)	6V23	3.1E−09	1.1	24.6	5.9	69.5
		8V5	5.5E−09	1.2	17.9	11.5	70.7
		4V21	5.1E−08	1.1	13.9	4.1	82.0
		6V3	5.5E−08	1.0	8.2	3.9	87.9
		8V7	1.5E−09	21.7	2.0	1.5	96.6
		6V20	2.4E−08	17.1	3.6	1.4	95.0
		3V7	7.5E−07	18.6	0.1	0.4	99.5
		6V9	3.3E−08	39.7	1.3	0.4	98.4
		6V1	5.5E−08	40.8	0.5	0.6	98.8
Air 30% steam 80 °C	Silver (22 cm^2)	8V28	4.8E−10	1.2	0.0	0.0	100.0
		6V25	4.1E−09	1.5	7.9	0.8	91.3
		4V12	1.8E−08	1.1	4.0	0.0	96.0
		8V37	9.8E−10	13.1	0.0	0.0	100.0
		3V8	7.5E−07	17.3	0.0	0.4	99.7
O_2 30% steam 80 °C	Steel (3 cm^2)	5V23	3.7E−08	1.4	21.1	77.7	1.3
		6V27	9.8E−09	1.2	9.5	89.1	1.4
		6V32	6.3E−09	15.3	0.0	98.3	1.7
		9V22	3.3E−09	16.2	1.2	91.9	7.0
O_2 30% steam 80 °C	Silver (22 cm^2)	6V29	7.4E−09	1.3	2.6	0.8	96.6
		5V21	4.0E−08	1.2	11.4	1.8	86.8
		5V17	8.3E−08	16.8	14.0	25.2	60.8
O_2 30% steam 80 °C	Paint (5 cm^2)	5V20	4.0E−08	1.0	21.5	14.6	63.8
		6V6	2.1E−08	1.0	24.2	4.7	71.1
		6V28	9.8E−09	1.0	15.6	3.8	80.7
		5V18	8.3E−08	14.7	11.2	44.1	44.7
		6V5	2.1E−08	18.8	9.6	1.2	89.2
		6V33	6.3E−09	20.7	3.5	0.0	96.5
Air + steam + H_2 + steel at 80 °C	Steel (3 cm^2)	4V28	3.4E−08	1.2	88.8	10.1	1.1
		11T14	1.8E−08	16.3	77.2	22.3	0.5
Air 30% steam 4% H_2 80 °C	Paint (5 cm^2)	4V26	3.4E−08	1.1	26.5	7.1	66.4
		4V17	7.2E−08	13.5	5.2	2.7	92.1
Air 30% steam 4% H_2 80 °C	Silver (22 cm^2)	4V29	3.4E−08	1.0	4.6	0	95.4
		4V19	4.7E−08	13.3	2.8	4.3	93.0
Air 30% steam 130 °C	–	8V23	9.1E−10	2.4	85.8	14.2	–
		8V32	1.6E−09	25.2	24.9	75.1	
		8V33	1.6E−09	18.3	64.3	35.7	
Air 30% steam 130 °C	Paint (4 cm^2)	8V29	1.1E−09	2.0	4.8	2.5	92.7
		8V30	1.1E−09	1.5	14.4	1.6	84.0
		8V35	9.8E−10	19.1	0.0	0.0	100.0
		8V36	9.8E−10	20.2	0.0	0.0	100.0

to a pre-existing flaw, such as pitting could be one reason for this observation, increased IO_x deposition on the steel surface in these tests can also not be ruled out.

No iodine speciation was performed on the steel coupons at these very low loadings. For the modelling, the small iodine deposition could have resulted from I_2 adsorption or from settling of IO_x. Additionally, adsorbed I_2 could have been subsequently oxidised into IO_x by ARP.

In an O_2/steam atmosphere (Fig. 13), very little iodine is adsorbed onto the steel surface, as observed in an air/steam atmosphere. This means that the I_2 adsorption kinetics are very slow compared to I_2/IO_x conversion kinetics in these conditions. Moreover, the conversion of I_2 into IO_x is almost complete even for low adsorbed doses. This is consistent with the results displayed in Fig. 5 in the absence of steel.

In an air/steam/H_2 atmosphere and in the presence of a steel surface, only two tests at different doses were performed (Fig. 14). The amount of iodine deposited on the steel on these experiments is negligibly small. The I_2/IO_x conversion result is the same as that obtained without a steel surface (Fig. 6), very little I_2 is converted into IO_x. H_2 seems to reduce the oxidising power of the irradiated atmosphere.

5.2.2. Modelling

An example of the modelling of iodine chemistry in presence of steel is shown in Fig. 15 for the air/steam atmosphere as it is the most representative case. The initial concentration of iodine was set at 4×10^{-8} mol L^{-1}, in order to compare the calculations with relevant experimental data. For a stainless steel surface, several studies are found in the literature Wren et al. (1999). Evans and Nugraha (2002), Wren and Glowa (2001) and Funke et al. (1996a). It appears that the iodine adsorption constant depends on the quality of steel and on the humidity. However, for 316L stainless steel, an order of magnitude of about 1×10^{-5} m s^{-1} is considered as a representative value. For the iodine desorption constant, a relevant and representative value for 316L stainless steel is about 1×10^{-7} s^{-1} according to Evans and Nugraha (2002). That is why an adsorption constant of 1×10^{-5} m s^{-1} was chosen for the modelling of these tests. For the same reasons, the desorption constant was set at 1×10^{-7} s^{-1}.

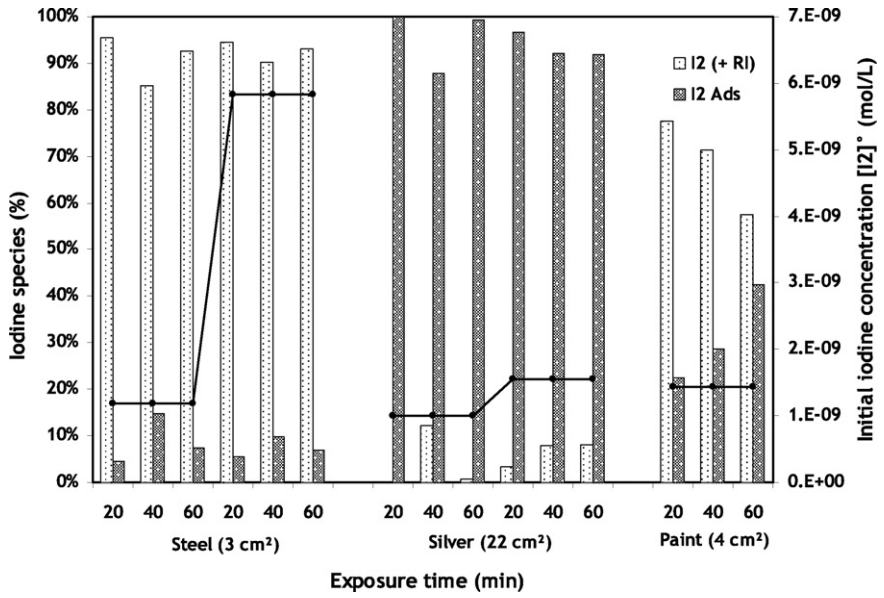

Fig. 11. Relative speciation (histograms, left axis) of iodine species at 130 °C in air/steam 30% mixture when surfaces are introduced in the glass vessel as a function of time and initial I_2 concentration (full black lines, right axis) (no irradiation; no iodine oxides are considered to be formed in these experiments).

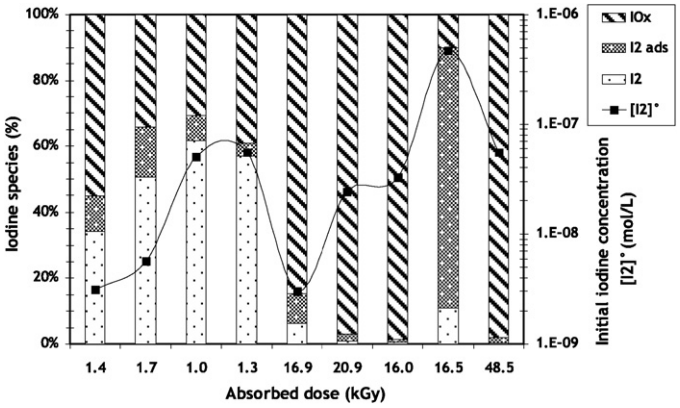

Fig. 12. Relative speciation of iodine species at 80 °C in air/steam 30% mixture when a steel coupon (3 cm^2) is introduced in the glass vessel as a function of adsorbed dose and initial I_2 concentration (dose rate close to 1 kGy h^{-1}).

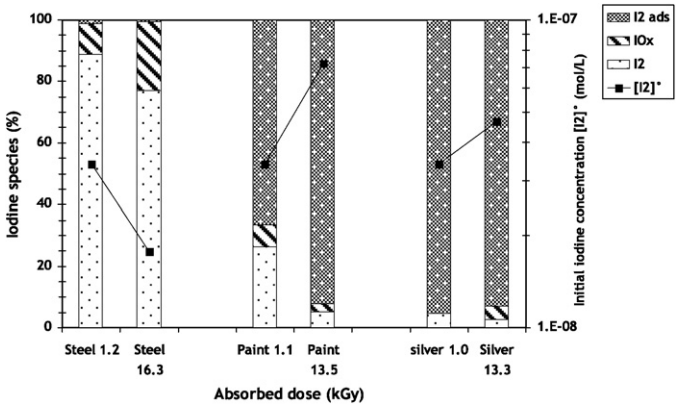

Fig. 14. Relative speciation of iodine species at 80 °C in air/steam (30%)/H_2 (4%) mixtures when a steel coupon (3 cm^2), painted coupon (5 cm^2) or a silver coupon (22 cm^2) is introduced in the glass vessel as a function of adsorbed dose and initial I_2 concentration (dose rate close to 1 kGy h^{-1}).

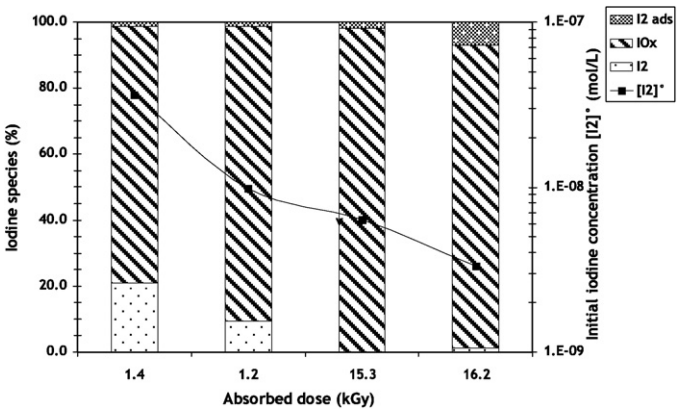

Fig. 13. Relative speciation of iodine species at 80 °C in O_2/steam 30% mixture when a steel coupon (3 cm^2) is introduced in the glass vessel as a function of adsorbed dose and initial I_2 concentration (dose rate close to 1 kGy h^{-1}).

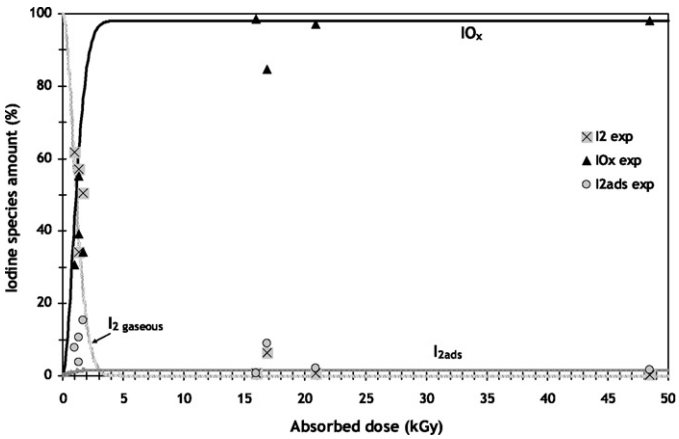

Fig. 15. Evolution of the relative amount of modelled iodine oxides, gaseous I_2 and adsorbed iodine onto steel at 80 °C as a function of absorbed doses and comparison with all experimental data (except at 16.5 kGy) for an air/steam 30% mixture and a steel surface of 3 cm^2 ($[I_2]°_{exp}$ close to 4×10^{-8} mol L^{-1}, dose rate close to 1 kGy h^{-1}, $[I_2]°_{modelling} = 3 \times 10^{-8}$ mol L^{-1}).

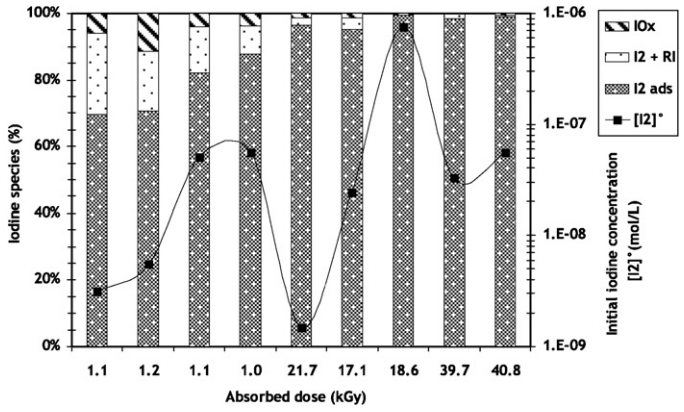

Fig. 16. Relative speciation of iodine species at 80 °C in air/steam 30% mixture when a painted coupon (5 cm^2) is introduced in the glass vessel as a function of adsorbed dose and initial I_2 concentration (dose rate close to 1 kGy h^{-1}).

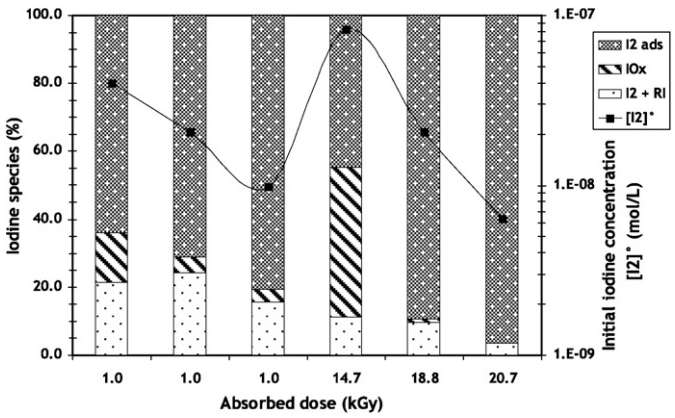

Fig. 17. Relative speciation of iodine species at 80 °C in O_2/steam 30% mixture when a painted coupon (5 cm^2) is introduced in the glass vessel as a function of adsorbed dose and initial I_2 concentration (dose rate close to 1 kGy h^{-1}).

Except the test at 16.5 kGy (initial I_2 concentration higher than 1×10^{-7} mol L^{-1}), the initial I_2 concentration is not an important parameter according to Fig. 12. As a consequence, all these experimental results were compared to the modelling results irrespective of the initial concentration as long as it was below 1×10^{-7} mol L^{-1}.

Fig. 15 shows that the experimental results are quite well reproduced by the model for iodine oxides, gaseous I_2 and adsorbed I_2. Although the measurements were performed only at 2 doses, the transition from zero to almost complete conversion into IO_x was observed experimentally, as was the long-term stationary iodine speciation at steady-state. The very small amount of adsorbed iodine observed in the experiments is also predicted by the model. Even if approximate, a refinement of the kinetics constants of iodine interaction with steel is not necessary for these tests as adsorbed iodine is well reproduced and is of secondary importance in these tests (few percent in comparison with iodine oxides that are the main products formed). The model presented in Section 3 is sufficient to describe iodine behaviour in an irradiated air/steam atmosphere and in the presence of stainless steel. However, the few experimental data in these conditions are not suitable to allow firm conclusions about the model. In fact, chemistry between steel and iodine is much more complex (Wren et al., 1999; Wren and Glowa, 2001) and physisorption is accompanied by a significant chemisorption with different stoichiometries in the I–Fe–O system as illustrated in Fig. 3 (left part). The subsequent evaporation behaviour of iodine is also not well known. More experimental data would be needed to confirm the reliability of the modelled kinetics, but also more modelling considerations would be necessary to describe and reproduce in details iodine chemistry onto steel surfaces during irradiation.

5.3. Painted surface

5.3.1. Experimental results

Fig. 16 shows the iodine speciation after irradiation in air/30% steam at 80 °C and in the presence of a painted coupon. The majority of the iodine is trapped onto paint, indicating that adsorption of I_2 onto paint is faster than formation of IO_x by reaction of I_2 with ARP. The I_2 nearly behaves as if there had been no irradiation.

The strength of I_2 adsorption onto paint is rationalised by the strong affinity of iodine towards chemical groups in the components of an epoxy paint (amines, amides and hydroxyl groups) (Powers and Salay, 2009; Bosland et al., 2010b; Bosland, 2009). It is known since many years that iodine creates strong bonding onto paint that may be desorbed slowly under I_2 form (Dickinson et al., 1997, 2001a; Rosenberg et al., 1969; Sims et al., 1997) or release in an organic form (RI, with R an alkyl chain) under irradiation conditions (Funke, 1999; Guilbert et al., 2008; Baston et al., 1999; Deane, 1989, 1991; Dickinson et al., 2001b; Hellmann et al., 1996; Postma and Zadovski, 1972; Taghipour and Evans, 2000) as illustrated in Fig. 3 (right part).

The fraction of IO_x and volatile iodine species (I_2 and RI) seem to slightly decrease with adsorbed dose (Fig. 16). The radiolytic conversion of IO_x into gaseous compounds such as I_2 or RI could explain this apparent tendency, although this has never been previously observed. The produced I_2 would be adsorbed back onto the paint whereas the produced RI would be converted back into IO_x, resulting in an increased iodine loading in the long-term of irradiation. In fact, for the very long irradiation time, paint can be degraded by gamma rays and form gaseous organic compounds (R) that may react with IO_x compounds. Recently, studies of the radiolytic stability of IO_x were started in the EPICUR facility. The current OECD-BIP project with irradiations of about 200 h and a dose rate of about 2.5 kGy h^{-1} (Gauvain, 2007) will also contribute to a better understanding of the potential for this process.

There was no detectable effect of the initial iodine concentration in an air/steam atmosphere as shown in Fig. 16, even at high concentrations close to 1×10^{-6} mol L^{-1}. However, in an O_2/steam atmosphere at the same temperature (Fig. 17), iodine oxidation becomes significant at an initial iodine concentrations close to 1×10^{-7} mol L^{-1}. In such oxygen- and I_2-rich conditions, iodine oxidation can apparently compete kinetically with I_2 adsorption.

The influence of the temperature (130 °C) was studied for low iodine concentrations around 1×10^{-9} mol L^{-1} with no detectable effect on iodine speciation (Fig. 18). The main species at the end of the tests remains iodine adsorbed on the paint coupon.

No significant influence of H_2 is apparent when comparing data from Fig. 14 to that from Fig. 16.

Only small amounts of less than 5% of the iodine deposit on the painted coupon could be washed off after the irradiations. This suggests a strong affinity of iodine to the epoxy paint chemical groups, and would favour the assumption of a fast chemical reaction of I_2 with the paint, leading to strongly bound iodine at the large paint molecules. Deposits of IO_x particles formed by radiolysis in the gaseous phase would be expected to be washed off much easier. This means that the process "deposition of IO_x particles on the surface" as indicated in Fig. 4 is conceivable but obviously not significant in the PARIS tests.

5.3.2. Modelling

An example of the modelling of iodine behaviour in presence of paint in an air/steam mixture at 80 °C is shown in Fig. 19 for initial iodine concentration of 5×10^{-8} mol L^{-1}. As the initial I_2

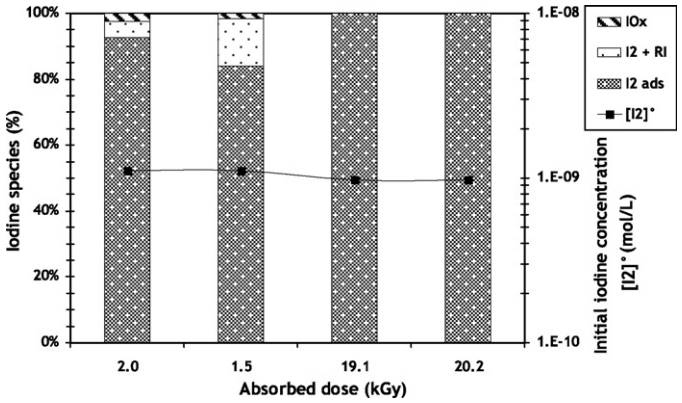

Fig. 18. Relative speciation of iodine species at 130 °C in air/steam 30% mixture when a painted coupon (4 cm^2) is introduced in the glass vessel as a function of adsorbed dose and initial I_2 concentration (dose rate close to 1 kGy h^{-1}).

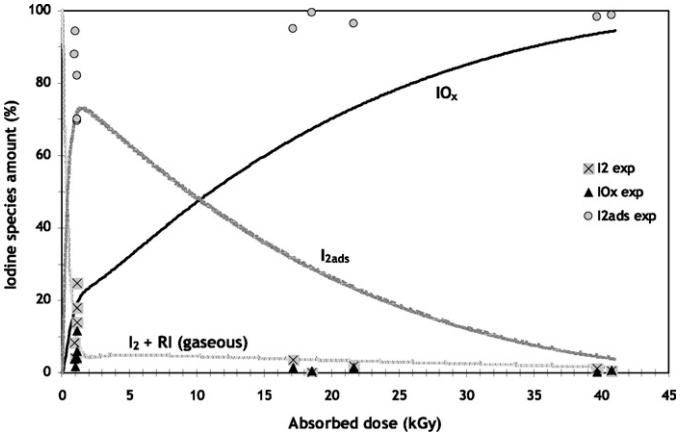

Fig. 19. Evolution of the relative amount of modelled iodine oxides, gaseous I_2 and adsorbed iodine at 80 °C as a function of absorbed doses and comparison with the experimental data for an air/steam 30% mixture and a painted surface of 4 cm^2 ($[I_2]°_{exp}$ comprised between 1×10^{-9} and 1×10^{-6} mol L^{-1} and dose rate close to 1 kGy h^{-1}, $[I_2]°_{modelling} = 5 \times 10^{-8}$ mol L^{-1}).

concentration is not a significant parameter according to Fig. 16, experimental results from tests with initial I_2 concentrations in the range 1×10^{-9} to 1×10^{-6} mol L^{-1} are compared to the modelling results. An adsorption constant close to 1×10^{-3} m s^{-1} was set for this paint type (epoxy) (Rosenberg et al., 1969; Baston and Sims, 2002; Zoulalian and Belval-Haltier, 1998, 2000) with a desorption constant close to 1×10^{-5} s^{-1} according to literature Rosenberg et al. (1969) and Barbe and Guilbert (2004) and own unpublished interpretation work.

The model calculation is in distinct disagreement with the experimental results. The main species at the end of the irradiation is calculated to be iodine oxides but measured to be iodine adsorbed on the paint. Several hypotheses to explain this discrepancy between experiment and model are discussed in the following.

The first hypothesis that iodine oxides were deposited onto the paint during the experiment (whereas this process is missing in the model) is ruled out because a substantial solubility of iodine deposits thus would have been expected from such an IO_x deposition, which is not consistent with the measured, small iodine solubility of the paint deposit. Moreover, as the paint surface is smaller than the glass surface, IO_x particles should have been deposed predominantly onto the glass, but actually, only a very low iodine amount was recovered from the glass or from the paint.

A second explanation could be related to the model of organic iodide formation which considers that all adsorbed iodine on the paint coupon can be released back into the gaseous phase as organic iodides (RI). Then, RI can be oxidised into IO_x, which are subsequently deposited onto surfaces. Physisorbed and chemisorbed iodine on the painted surface could also be oxidised by ARP into IO_x that would be stuck to the paint (instead of being deposited as suggested in the previous paragraph). This would result in the iodine remaining on the painted surface. As a consequence, the iodine loading on the painted surface would continuously increase in the experiment whereas the model predicts a decrease, as observed. It is known from other experimental data that iodine adsorbed on the painted surface is not significantly released (PHEBUS tests) (Gregoire et al., 2008; Hanniet and Repetto, 1999; Jacquemain et al., 2000; Payot et al., 2010). So, the total conversion of adsorbed I_2 into organic iodide seems to be overestimated in the modelling. The direct consequence is the radiolytic oxidation of these large amounts of RI into IO_x compounds as evidenced by the modelling results. In fact, iodine chemistry on the painted surfaces is rather difficult to understand and several chemical groups are involved in iodine trapping as mentioned in the previous section. All of them might not respond the same way to an irradiative stress. Some of them might form volatile organic iodides and other might be not affected. That is why the model of formation of organic iodides from painted surfaces probably overestimates the amount of RI that can be formed and has to take into account these mechanistic considerations. Another model of formation of organic iodides is under development based on EPICUR and BIP tests, considering these phenomena based on a literature review (Bosland, 2009). EPICUR and BIP data will also help to develop this model.

A third explanation is based upon the hypothesis that the radiolytic I_2 oxidation is actually slower in the PARIS test conditions than in the SIEMENS test conditions (Funke et al., 1999). Initial I_2 concentrations were higher in the SIEMENS tests by orders of magnitude, and the actual reaction mechanism of IO_x formation could therefore be different in the two test series including different overall IO_x formation rates. Dickinson's consistent analysis of the short term irradiations of both test series assuming a zeroth order IO_x formation mechanism (Dickinson and Sims, 2007) revealed that the zeroth order IO_x formation rate was slower in the PARIS test conditions than in the SIEMENS test conditions by about a factor of 10. This was rationalised by different reaction mechanisms in the different concentration regimes of both test series.

A fourth approach to explain the overestimation of IO_x formation is based upon post-test calculations of the iodine behaviour in PHEBUS test FPT1 using COCOSYS/AIM (Bosland et al., in press). In these calculations, the IO_x formation model based upon the SIEMENS tests had to be slowed down significantly in order to reproduce the correct iodine concentrations in the PHEBUS FPT1 gaseous phase which are closer to the concentration regime studied in the PARIS tests. This slowdown of IO_x formation was achieved in these calculations by significantly increasing the reaction rate between ozone and paint, thus significantly decreasing the ozone concentration and thus significantly decreasing the reaction partner for I_2 to produce IO_x.

5.4. Silver surface

5.4.1. Experimental results

Fig. 20 shows the speciation at the end of the irradiation in the presence of a silver coupon in air/30% steam atmosphere at 80 °C. Iodine exhibits a very strong affinity for silver as more than 95% of the initial iodine is bound to the surface, independent of the absorbed dose and initial iodine concentration. Very few amounts of iodine oxides were recovered, similar to the non-irradiated tests (Fig. 10). No influence of H_2 is evidenced with Fig. 14 as the adsorption process remains the main significant phenomena observed within the range of initial concentrations studied.

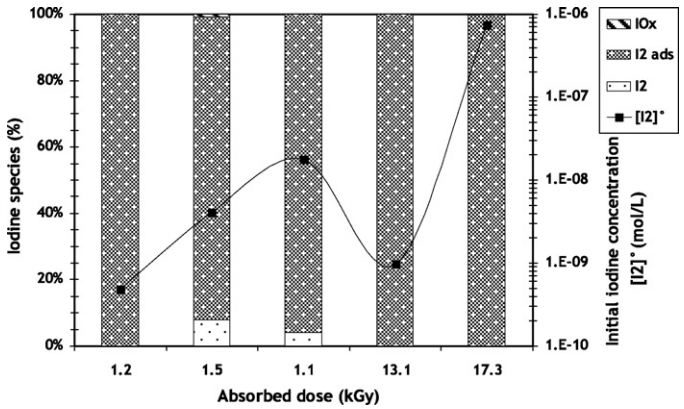

Fig. 20. Relative speciation of iodine species at 80 °C in air/steam 30% mixture when a silver coupon (22 cm^2) is introduced in the glass vessel as a function of adsorbed dose and initial I_2 concentration (dose rate close to 1 kGy h^{-1}).

In an O_2/steam atmosphere, when the initial concentration increases up to about 1×10^{-7} mol L^{-1}, I_2 adsorption decreases and IO_x formation and residual I_2 fractions become significant (Fig. 21). This observation is similar to what had been observed in the corresponding system with painted surfaces (Fig. 17).

Only minor amounts of the adsorbed iodine could be washed off from the Ag surface, suggesting that I_2 adsorption onto the Ag surface followed by chemisorption with formation of non-soluble AgI was the relevant process to produce the observed strong bond of iodine to the Ag surface.

In the air/steam conditions, the non-adsorbed iodine is recovered mainly as gaseous iodine. Practically no iodine oxides are detected in the vessel after removal of the Ag coupon. However, these limited observations should not be interpreted such that no iodine oxides were formed. This is because a small amount of IO_x could have been formed and subsequently settled down onto the Ag coupon surface during the test. Furthermore assuming that non-oxidised I_2 was not adsorbed onto the Ag surface at the same extent, the observation of a residual I_2 fraction being larger than the residual IO_x amount would also be explainable.

The kinetics of I_2 adsorption onto silver seems to be faster than radiolytic oxidation of I_2, as was observed with painted surfaces and for the non-irradiation tests. In aqueous systems the strong interaction of iodine with silver was already studied (Krausmann and Drossinos, 1999; Dickinson, 1997; Funke et al., 1996b; Jacquemain et al., 1996). In gaseous systems, interaction of Ag aerosols with I_2 at primary system temperatures far above the containment temperatures was performed (Beard et al., 1988). The present PARIS

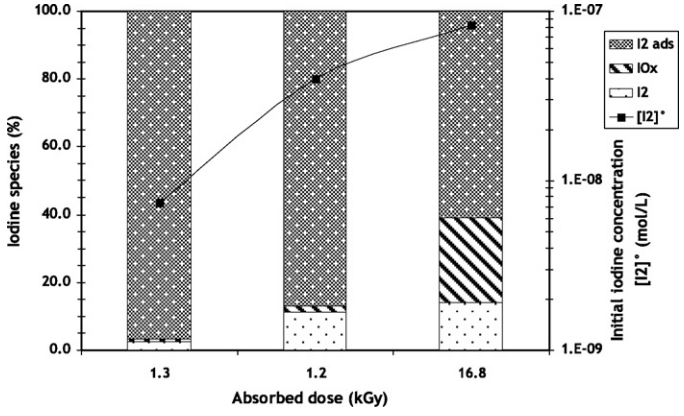

Fig. 21. Relative speciation of iodine species at 80 °C in O_2/steam 30% mixture when a silver coupon (22 cm^2) is introduced in the glass vessel as a function of adsorbed dose and initial I_2 concentration (dose rate close to 1 kGy h^{-1}).

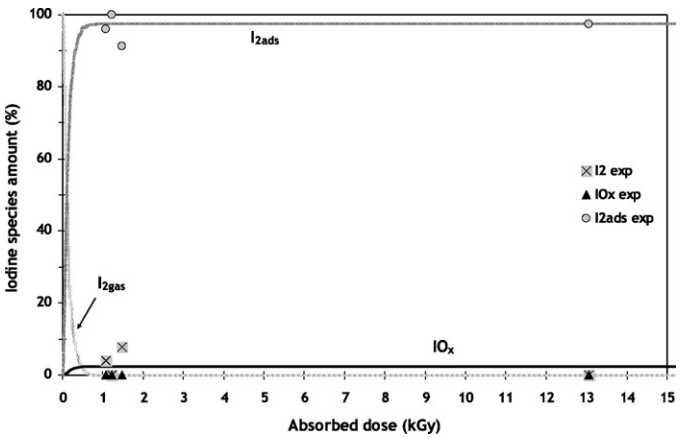

Fig. 22. Evolution of the relative amount of modelled iodine oxides, gaseous I_2 and adsorbed iodine at 80 °C as a function of absorbed doses and comparison with the experimental data for an air/steam 30% mixture and a silver surface of 22 cm^2 ($[I_2]°_{exp}$ comprised between 1×10^{-9} and 1×10^{-6} mol L^{-1}, dose rate close to 1 kGy h^{-1}, $[I_2]°_{modelling} = 1 \times 10^{-9}$ mol L^{-1}).

tests therefore fill a gap in the matrix of boundaries relevant to severe accidents. In fact, the obtained result of an effective I_2/Ag interaction in the containment atmosphere is very interesting for the safety studies performed in case of severe accident, because it represents an additional pathway to decrease the fraction of the gaseous iodine in containment. This is of particular interest in the short term, when FP and degradation materials including large amounts of Ag from the control rods are arriving into the containment mainly in aerosol form and represent large surface areas for I_2 adsorption. However, the specific Ag surface in this boundary condition can at present only be estimated to a value of 300 m^2 kg^{-1} as commonly considered in containment codes (Bosland et al., 2010a) and has to be considered as a maximum due to the limited availability of silver within the aerosol. More studies would be needed to quantify the I_2/Ag interaction rate in case of representative aerosols obtained from evaporated control rod silver.

5.4.2. Modelling

Fig. 22 shows the effect of silver surface on gaseous I_2 during irradiation in an air/30% steam atmosphere at 80 °C and compares data with the model for an initial iodine concentration of 1×10^{-9} mol L^{-1}. As the initial I_2 concentration is not a significant parameter in the PARIS tests according to Fig. 20, all experimental results from Fig. 20 with initial I_2 concentrations ranging from 1×10^{-9} to 1×10^{-6} mol L^{-1} were included in the comparison in Fig. 22. An I_2/Ag adsorption rate constant of 1×10^{-3} m s^{-1} was set in order to reproduce a fast iodine trapping onto silver. This is the same rate constant as for paint in this paper. The majority of iodine mass was measured on the silver coupon, and this result is reproduced by the calculations. In the model, adsorbed iodine is considered to be irreversibly bound to the silver surface so that no secondary release reaction or desorption of once trapped iodine is taking place. The trapping of iodine onto silver surface is so efficient that iodine oxides have no time to be produced in the vessel even at high iodine concentrations (1×10^{-6} mol L^{-1}). These tendencies are well modelled by the phenomenological model used in this work, even if more complex mechanisms may exist onto silver surface, as for steel.

5.5. Additional tests

5.5.1. Experimental results

Finally, some tests were performed with 2 types of surfaces in the vessel. Paint and silver surfaces were put at the same time under

Table 8
Summary of experimental data on radiolytic conversion of molecular iodine into iodine oxides (IO_x) in the presence of both type of surfaces at the same time.

Test conditions	Surface type	Test name	$[I_2]^\circ$ (mol L^{-1})	Dose (kGy)	Gaseous RI + I_2 (%)	IO_x (%)	Adsorbed I_2 onto silver surface (%)	Adsorbed I_2 onto paint surface (%)
Air 30% steam 80 °C	Silver (22 cm^2) + paint (4 cm^2)	4V11	1.8E−08	1.2	3.8	0.1	84.4	11.8
		4V8	5.7E−08	16.7	0.3	0.6	84.3	14.8
Air 30% steam 4% H_2 80 °C		4V30	3.4E−08	1.1	2.4	0.2	97.4	–
		4V18	7.2E−08	17.0	1.7	2.0	89.8	6.6

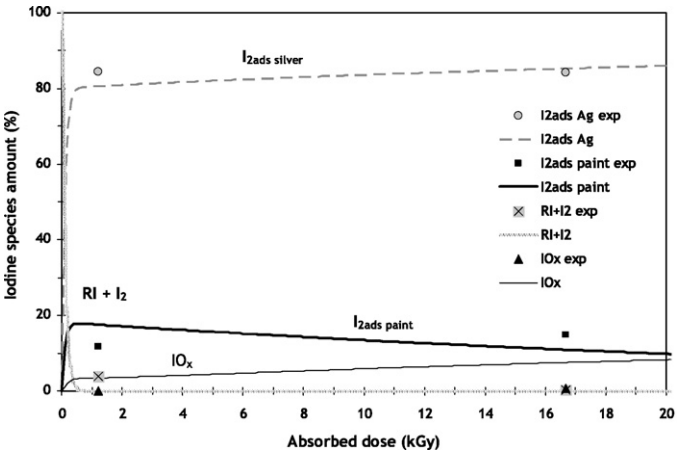

Fig. 23. Evolution of the relative amount of modelled iodine oxides, gaseous (RI + I_2) and adsorbed iodine at 80 °C as a function of absorbed doses and comparison with the experimental data for an air/steam 30% mixture and a silver surface of 22 cm^2 plus a paint surface of 4 cm^2 ($[I_2]^\circ_{exp\ and\ modelling}$ close to 3×10^{-8} mol L^{-1} and dose rate close to 1 kGy h^{-1}).

irradiation with the objective to validate the previously developed model. Table 8 summarizes these data. The majority of the iodine is trapped onto the silver surface as it is the larger surface in the vessel (22 cm^2 compared with 4 cm^2 for paint). As for the previous silver surface tests (Fig. 20), very low amounts of iodine oxides and remaining I_2 are measured, independent of the presence of hydrogen. The influence of paint on iodine volatility in these tests is low, as only about 10% are found on its surface.

5.5.2. *Modelling and validation of the models*

Fig. 23 shows the modelling of the evolution of gaseous I_2 versus the absorbed dose in an air/steam (30%) mixture at 80 °C and compares it to the experimental data for an initial I_2 concentration close to 3×10^{-8} mol L^{-1}. Iodine adsorption onto silver and paint is well reproduced all along the test. The IO_x amount is overestimated, which might be explained by the shortcomings in the model of RI formation from paint as mentioned in Section 5.3.2: even if small amounts of iodine are found onto the paint as compared with silver, the model of RI formation probably overestimates the IO_x formation. Finally, in these tests, silver governs mainly the iodine volatility. The discrepancies evidenced in Section 5.3.2 for paint are still present even if less significant due to the limited amount of iodine trapped by paint. However, this confirms the need for refining the RI formation model from painted surfaces by mechanistic considerations.

6. Conclusions

The PARIS project substantially enlarged the experimental database on radiolytic conversion of molecular iodine into iodine oxides under conditions relevant to severe accident containment atmospheres. Around 200 irradiated tests were performed in a number of different boundary conditions, without or including surface types representative for LWR containments.

From the tests in air/30% steam atmospheres, at initial iodine concentrations below 1×10^{-7} mol L^{-1}, and in the absence of LWR-representative surfaces, the conversion of I_2 into iodine oxides was shown to be almost complete for doses of about 20 kGy. At higher initial I_2 concentrations, this conversion is only partial. Oxygen promotes the iodine oxides formation through the increase of oxidising air radiolytic products. Doses of about 15 kGy are sufficient to convert the majority of initial I_2 into iodine oxides in O_2/30% steam atmospheres. Hydrogen exhibits the opposite effect, decreasing effect on IO_x formation, as it reduces the oxidation potential of the irradiated atmosphere. Temperature variation from 80 °C up to 130 °C did not provide a significant impact on the IO_x formation.

Calculations using an empirical model reproduce the main effect of radiolytic conversion of I_2 into IO_x, although the empirical model is not able to reproduce detailed differences in the boundary conditions. Furthermore, the evolution of I_2/IO_x conversion was measured in the PARIS tests only at two limited dose ranges. Quantitative model development of IO_x formation kinetics would require measuring the dose dependency in more detail. A direct determination of the radiolytic stability of IO_x remains an open question also from the current analysis of the PARIS test results, and this question is currently investigated in the frame of the EPICUR project.

The influence of steel surfaces, paint surfaces and silver surfaces on iodine radiochemistry was studied in the PARIS tests using ratios of surface to volume as representative for LWR and PHEBUS-FP containments. In case of silver, this was to simulate a conceivable effect of aerosols containing silver on the radiolytic I_2/IO_x conversion.

Stainless steel turned out to be no efficient trap for iodine, and so the majority of the iodine was converted into iodine oxides in these tests, nearly as if no stainless steel surfaces were present. These experimental results are well reproduced by empirical model, even only taking into account a simple, reversible iodine adsorption model. A more complex iodine chemistry is known to proceed on steel surfaces, but the competition between I_2 deposition onto the steel surface and the radiolytic conversion of I_2 into IO_x is obviously already sufficiently modelled with the simple iodine/steel model.

Painted surfaces were efficient traps for I_2, to such an extent that, in an air/steam atmosphere at initial I_2 concentrations below 1×10^{-7} mol L^{-1}, the radiolytic oxidation of iodine in the gaseous phase is largely suppressed. Only at higher initial I_2 concentrations, radiolytic IO_x formation seems to compete with I_2 adsorption. Contrary to the experimental data the model predicts a dominant IO_x formation at higher doses. Qualitative explanations are at hand: (i) the IO_x formation rate is modelled too fast in the low I_2 concentration regime of the PARIS tests, (ii) the model of organic iodide formation and a subsequent release into the gaseous phase is too efficient and the model unrealistically enriches organic iodide in the gaseous phase, that are then destructed into iodine oxides by irradiation. Mechanistic considerations are under consideration in order to develop a new model of release of RI from a loaded painted coupon. EPICUR (Guilbert et al., 2008, 2007) and BIP (Gauvain, 2007) tests are currently performed by IRSN (France) and AECL (Canada) within the ISTP and OECD programmes, respectively. They will constitute the experimental database to develop and validate a new model. SARNET (Severe Accident Research NETwork) 1 programme (Haste et al., 2009; Micaelli et al., 2006) was partly devoted to the analysis of the radiolytic oxidation of

iodine in containment. SARNET 2 programme (Albiol et al., 2008) will also be devoted to an analysis of the data provided by both projects and the associated developed models on iodine chemistry in the containment, particularly on organic iodides release from painted surfaces under irradiation.

Silver surfaces represented an effective I_2 trap in the PARIS tests, similar to the painted surfaces. Unlike the painted surfaces, the model calculation successfully reproduces the experimental iodine partitioning between gaseous phase and surface, whereas iodine deposited on the silver surface is dominating. Radiolytic formation of iodine oxides was a subordinate process in the presence of silver.

Although a large number of irradiated iodine tests were performed during the PARIS project, the numerous experimental parameters and their study did not allow to perform a sufficient number of repeating tests in order to reduce the large data scattering. More parameter effects are suspected to exist in the field of radiolytic I_2/IO_x conversion, but these could not be identified under the given conditions. To further validate the radiolytic I_2 oxidation model implemented in severe accident codes such as ASTEC some experiments are currently performed on iodine oxides formation to measure IO_x speciation and characterisation in order to identify in a more precise way their stoichiometry. In order to better quantify the real impact of silver on iodine radiochemistry, more representative conditions should be established by replacing the silver foils in the PARIS project with multi-component aerosols containing silver.

Acknowledgement

We thank F. Payot (IRSN) for his contribution to the preliminary interpretation of the results.

References

Albiol, T., van Dorsselaere, J.P., Tromm, W., Journeau, C., Kljenak, I., Haste, T., Sehgal, B., Beraha, D., 2008. Presentation of SARNET2. In: Proceedings of the 3rd European Review Meeting on Severe Accident Research (ERMSAR 2008) , Nesseber, Bulgaria, 23–25 September.

Allelein, H.J., Neu, K., van Dorsselaere, J.P., Müeller, K., Kostka, P., Barnak, M., Matejovic, P., Bujan, A., Slaby, J., 2003. European validation of the integral code ASTEC (EVITA). Nucl. Eng. Des. 221, 95–118.

Allelein, H.J., Neu, K., van Dorsselaere, J.P., 2005. European validation of the integral code ASTEC (EVITA) – first experience in validation and plant sequence calculations. Nucl. Eng. Des. 235, 285–308.

Allelein, H.J., Arndt, S., Klein-Hessling, W., Schwarz, M., Spengler, C., Weber, G., 2008. COCOSYS: status of development and validation of the German containment code system. Nucl. Eng. Des. 238 (4), 872–889.

Aubert, F., 2002. Destruction par radiolyse gamma de l'iodure de methyl en faible concentration dans l'air humide. Thesis. Université d'Aix-Marseille III, France.

Barbe, C., Guilbert, S., 2004. Etude de la fixation et de la désorption de l'iode moléculaire sur des films de peinture. IRSN.

Baston, G.M.N., Sims, H.E., 2002. The reaction of gaseous iodine with steel and paint surfaces. EPRI Report ACEX Project TR C-41.

Baston, G.M.N., Deane, A.M., Dickinson, S., Freemantle, N.E., Matcham, A.J., Sims, H.E., 1999. Radiolytic production of organic iodine. Part II: formation on painted surfaces. In: European Community Report ST-OIC(98)12, AEA Technology Report AEAT-4541 Issue 2.

Beard, A.M., Bowsher, B.R., Nichols, A.L., 1988. Interaction of the molecular iodine vapour with silver–indium–cadmium control rod aerosol. In: Proceedings: Severe Accident in Nuclear Power Plants , 21–25 March, Sorrento, Italy.

Bell, J.T., Lietzke, M.H., Palmer, D.A., 1982. Predicted rates of formation of iodine hydrolysis species at pH levels, concentrations and temperatures anticipated in LWR accidents. In: NUREG/CR – 2900, ORNL – 5876.

Bosland, L., 2009. Towards a better understanding of the mechanisms of paint ageing and volatile iodine (I_2, CH_3I HI) and volatile ruthenium (RuO_4) trapping – a litterature review. In: IRSN/DPAM/SEMIC – 2009-282.

Bosland, L., Funke, F., Girault, N., Langrock, G., 2008. PARIS project: Radiolytic oxidation of molecular iodine in containment during a nuclear reactor severe accident. Part 1. Formation and destruction of air radiolysis products – experimental results and modelling. Nucl. Eng. Des. 238 (12), 3542–3550.

Bosland, L., Cantrel, L., Girault, N., Clement, B., 2010a. Modelling of iodine radiochemistry in the ASTEC severe accident code: description and application to FPT-2 PHEBUS test. Nucl. Technol. 171 (1), 88–107.

Bosland, L., Colombani, J., Simondi-teisseire, B., Powers, D.A., Dickinson, S., Girault, N., Clement, B., 2010b. Towards a mechanistic interpretation of iodine and paint interactions. In: Proceedings of the 4rd European Review Meeting on Severe Accident Research (ERMSAR 2010) , Bologne, Italy, 10–12 May, p. 2010.

Bosland, L., Weber, B., Klein-Hessling, W., Girault, N., Clement, B. Modelling and interpretation of iodine behaviour in PHEBUS FPT-1 containment with ASTEC and COCOSYS codes. Nucl. Technol., in press.

Clement, B., Hanniet, N., Repetto, G., Jacquemain, D., Jones, A.V., Kissane, M.P., von der Hardt, P., 2003. LWR severe accident simulation: synthesis of the results and interpretation of the first PHEBUS FP experiment FPT-0. Nucl. Eng. Des. 226, 5–82.

Cousin, F., Dieschourg, K., Jacq, F., 2008. New capabilities of simulating fission product transport in circuits with ASTEC/SOPHAEROS v.1.3. Nucl. Eng. Des. 238 (9), 2430–2438.

Deane, A.M., 1989. Organic iodine formation rates on surfaces in pressurised water reactor buildings. AEA Report AERE-R 13526.

Deane, A.M., 1991. Volatile organic iodide formation by surface processes. In: Proceedings of the Third CSNI Workshop on Iodine Chemistry in Reactor Safety , Tokai-Mura, Japan, September 11–13.

Dickinson, S., 1997. Modelling of iodine/silver reactions. In: AEAT Report ST-IC/P, vol. 97, no. 18.

Dickinson, S., Sims, H.E., 2000. Development of Inspect model for the prediction of iodine volatility from irradiated solutions. Nucl. Technol. 129 (3), 374–386.

Dickinson, S., Sims, H.E., 2007. Network of Excellence For A Sustainable Integration Of European Research On Severe Accident Phenomenology, Iodine Data Book Part 5: Gaseous Iodine Chemistry. SARNET-ST-P50 – WMT(06)P081.

Dickinson, S., Sims, H.E., Belval-Haltier, E., Jacquemain, D., Poletiko, C., Funke, F., Drossinos, Y., Krausmann, E., Herrero, B., Routamo, T., Handy, B.J., 1997. Iodine chemistry. In: Proc. FISA-97 Symp. on EU Research on Severe Accident – EUR 18258 EN, 232 , Luxembourg, November 17–19.

Dickinson, S., Sims, H.E., Funke, F., Bruchertseifer, H., Liljenzin, J.O., Liger, K., Montanelli, T., Krausmann, E., Rydl, A., 2001a. Iodine chemistry and mitigation mechanisms (ICHEMM). In: FISA-2001.

Dickinson, S., Sims, H.E., Belval-Haltier, E., Jacquemain, D., Poletiko, C., Funke, F., Hellmann, S., Karjunen, T., Zilliacus, R., 2001b. Organic iodine chemistry. Nucl. Eng. Des. 209, 193–200.

Dickinson, S., Baston, G.M.N., Sims, H.E., Funke, F., Cripps, R., Bruchertseifer, H., Jäckel, B., Guentay, S., Glänneskog, H., Liljenzin, J.O., Cantrel, L., Kissane, M., Krausmann, E., Rydl, A., 2003. Iodine chemistry and mitigation mechanisms: ICHEMM final synthesis report. In: EC, 5th Euratom Framework Programme 1998–2002, FIKS-CT1999-00008.

Evans, G., Nugraha, T., 2002. A study of the kinetics of I_2 deposition on stainless steel sampling lines. Nucl. Technol. 140 (3), 315–327.

FACSIMILE, 2008. FACSIMILE, v.4.0 User Guide, MCPA Software, www.mcpa-software.com.

Filistovic, V., Nedveckaite, T., 1999. Photochemical aspects of the behaviour of the atmospheric radioiodine after the Chernobyl accident. J. Radioanal. Nucl. Chem. 242 (1), 75–80.

Funke, F., 1999. Data analysis and modelling of organic iodide production at painted surfaces. In: OECD Workshop on Iodine Aspects of Severe Accident Management , Vantaa, Finland, May 18–20, pp. 151–168.

Funke, F., Greger, G.U., Hellmann, S., Bleier, A., Morell, W., 1996a. Iodine–steel reactions under severe accident conditions in light-water reactors. Nucl. Eng. Des. 166, 357–365.

Funke, F., Greger, G.U., Bleier, A., Hellmann, S., Morell, W., 1996b. The reaction between iodine and silver under severe PWR accident conditions. An experimental parameter study. In: Proceedings of the 4th CSNI Workshop on the Chemistry of Iodine in Reactor Safety – NEA/CSNI/R(96) 6 , Würelingen, Switzerland, June 10–12, p. 283.

Funke, F., Zeh, P., Hellmann, S., 1999. Radiolytic oxidation of molecular iodine in the containment atmosphere. In: OECD Workshop on Iodine Aspects of Severe Accident Management , Vantaa, Finland, May 18–20, pp. 79–89.

Funke, F., Langrock, G., Kanzleiter, T., Poss, G., Fischer, K., Kühnel, A., Weber, G., Allelein, H.J. Iodine oxides in large-scale THAI tests. Nucl. Eng. Des., submitted for publication.

Gauvain, J., 2007. Minutes of the first meeting of the programme review group of the OECD-NEA BIP Project. OECD/NEA – BIP PRG/Sec/(07)1.

Girault, N., Dickinson, S., Funke, F., Auvinen, A., Herranz, L., Krausmann, E., 2006. Iodine behaviour under LWR accident conditions: lessons learnt from analyses of the first two PHEBUS FP tests. Nucl. Eng. Des. 236 (12), 1293–1308.

Girault, N., Fiche, C., Bujan, A., Dienstbier, J., 2009. Towards a better understanding of iodine chemistry in RCS of nuclear reactors. Nucl. Eng. Des. 239 (6), 1162–1170.

Gregoire, A.C., March, P., Payot, F., Ritter, R., Zabiego, M., de Bremaecker, A., Biard, B., Gregoire, G., Schlutig, S., 2008. FPT-2 final report. IRSN/DPAM/DIR 2008 – 272 – Report PHEBUS-FP IP/08/579.

Guilbert, S., Bosland, L., Jacquemain, D., Clement, B., Andreo, F., Ducros, G., Dickinson, S., Herranz, L., Ball, J., 2007. Radiolytic oxidation of iodine in the containment at high temperature and dose rate. In: International Conference on Nuclear Energy for New Europe (NENE) , September 10–13, Portorose, Slovenia.

Guilbert, S., Bosland, L., Fillet, S., Jacquemain, D., Clement, B., Andreo, F., Ducros, G., Dickinson, S., Herranz, L.E., Ball, J., 2008. Formation of organic iodide in the containment in case of a severe accident. In: American Nuclear Society Annual Meeting , June 08–12, Anaheim, United States.

Hanniet, N., Repetto, G., 1999. FPT-0 final report. CEA/IPSN/DRS/SEA/PEPF – Report PHEBUS PHPF IP/99/423.

Haste, T., Giordano, P., Herranz, L., Girault, N., Dubourg, R., Sabroux, J.C., Cantrel, L., Bottomley, S., Parozzi, F., Auvinen, A., Dickinson, S., Lamy, J.C., Weber, G., Albiol, T., 2009. SARNET integrated European severe accident research – conclusions in the source term area. Nucl. Eng. Des. 239 (12), 3116–3131.

Hellmann, S., Funke, F., Greger, G.U., Bleier, A., Morell, W., 1996. The reaction between iodine and organic coatings under severe PWR accident conditions – an experimental study. In: Proc. 4th CSNI Workshop on the Chemistry of Iodine in Reactor Safety, NEA/CSNI/R(96)6 , June 10–12, Würelingen, Switzerland, p. 345.

Jacquemain, D., Poletiko, C., Chuaqui, C.A., 1996. Silver/iodine interactions under reactor accident conditions. In: Proceedings of the International Conference on Nuclear Containment , Cambridge, UK, September 23–25.

Jacquemain, D., Hanniet, N., Hueber, C., Poletiko, C., Chuaqui, C.A., Powers, D.A., Dickinson, S., Herrero, B., 1997. Overview of the iodine behaviour in PHEBUS FPT-0. In: Int. Conf. Nucl. Eng., ICONE , p. 201.

Jacquemain, D., Bourdon, S., Bremaecker, A., Barrachin, M., 2000. FPT-1 final report. CEA/IPSN/DRS/SEA/PEPF – Rapport SEA 1/100 – Report PHEBUS FP IP/00/479.

Kissane, M., 2008. On the nature of aerosols produced during a severe accident of a water-cooled nuclear reactor. Nucl. Eng. Des. 238, 2792–2800.

Krausmann, E., Drossinos, Y., 1999. A model of silver–iodine reactions in a light water reactor containment sump under severe accident conditions. J. Nucl. Mater. 264 (1–2).

Lin, C.C., 1980. Chemical behavior of radioiodine in BWR systems. J. Inorg. Nucl. Chem. 42 (8), 1093–1099.

Micaelli, J.C., Haste, T., van Dorsselaere, J.P., Bonnet, J.P., Meyer, J.M., Beraha, D., Annunzato, A., Chaumont, B., Adroguer, B., Sehgal, B., Trambauer, K., 2006. SARNET: a European cooperative effort on LWR severe accident research. In: Proceedings of the European Nuclear Society Meeting, vol. 1. Revue Générale Nucléaire, no. 1 , Paris, December 2005.

Narayanan, A., 2000. A global model for iodine behaviour in containment. Thesis. University of Toronto, Canada.

Payot, F., Haste, T., Biard, B., Bot-Robin, F., Devoy, J., Garnier, Y., Guillot, J., Manenc, C., March, P., 2010. FPT-3 final report. DPAM/DIR-2010-148 – PF IP/10/587.

Postma, A.K., Zadovski, R.W., 1972. Review of organic iodide. Formation under accident conditions in water-cooled reactors, United States Atomic Energy. Commission Report WASH-1233.

Powers, D.A., Salay, M., 2009. What is paint? In: UE PETTEN Center, Netherlands, 8th ISTP/CHEMIC Meeting, April 2nd.

Rosenberg, H.S., Genco, J.M., Morrison D.L., 1969. Fission product deposition and its enhancement under reactor accident conditions: deposition on containment system surfaces. Report BMI-1865, Battelle Memorial Institute, Ohio, United States.

Schwarz, M., Hache, G., von der Hardt, P., Phebus, F.P., 1999. A severe research programme for current and advanced light water reactions. Nucl. Eng. Des. 187, 47.

Schwarz, M., Clement, B., Jones, A.V., 2001. Applicability of PHEBUS FP results to severe accident safety evaluations and management measures. Nucl. Eng. Des. 209 (1–3), 173–181.

Simondi-Teisseire, B., 2008. Description of the PHEBUS FP programme. Trans. Am. Soc. 98, 267–269.

Sims, H.E., Dickinson, S., Evans, G., Wren, J.C., Glowa, G., 1997. Iodine behaviour in containment: the reaction of iodine with surfaces. In: Report AEA Technology – ACEX TR-B-06.

Sonnenkalb, M., Poss, G., 2009. The international test programme in the THAI Facility and its use for code validation. In: EUROSAFE Forum , November 2nd and 3rd, Sheraton Hotel, Brussels, Belgium.

Taghipour, F., Evans, G.J., 2000. Radiolytic organic iodide formation under nuclear reactor accident conditions. Environ. Sci. Technol. 34 (14), 3012–3017.

Tang, I.N., Castelman, A.W., 1970. Kinetics of induced decomposition of methyl iodide in air. J. Phys. Chem. 74 (22), 3933–3939.

van Dorsselaere, J.P., 2008. Applications of ASTEC integral code in the SARNET network. In: Proceedings of the International Conference on Nuclear Engineering, ICONE 16, May 11–15, Orlando, Florida, United States, vol. 3, pp. 369–379.

van Dorsselaere, J.P., Pignet, S., Seropian, C., Montanelli, T., Giordano, P., Jacq, F., Schwinges, B., 2005. Development and assessment of ASTEC CODE for severe accident simulation. In: 11th NURETH , Popes Palace Conference Center, Avignon, France, October 2–6.

van Dorsselaere, J.P., Seropian, C., Chatelard, P., Jacq, F., Fleurot, J., Giordano, P., Reinke, N., Schwinges, B., Allelein, H.J., Luther, W., 2009. The ASTEC integral code for severe accident simulation. Nucl. Technol. 165 (3), 293–307.

van Dorsselaere, J.P., Chatelard, P., Cranga, M., Guillard, G., Tregoures, N., Bosland, L., Brillant, G., Girault, N., Bentaib, A., Reinke, N., Luther, W., 2010. Validation status of the ASTEC integral code for severe accident simulation. Nucl. Technol. 170 (3), 397–415.

Vikis, A.C., MacFarlane, R., 1985. Reaction of iodine with ozone in the gas phase. J. Phys. Chem. 89, 812–815.

Weber, G., Bosland, L., Funke, F., Glowa, G., Kanzleiter, T., 2009. ASTEC, COCOSYS, and LIRIC interpretation of the iodine behaviour in the large-scale THAI test Iod-9. In: Proceedings of the 17th International Conference on Nuclear Engineering (ICONE17) , July 12–16, Brussels, Belgium, ICONE 17-75414, vol. 2, pp. 519–531.

Wren, J.C., Glowa, G.A., 2001. Kinetics of gaseous iodine uptake onto stainless steel during iodine-assisted corrosion. Nucl. Technol. 133 (1), 33–49.

Wren, J.C., Glowa, G.A., Meritt, J., 1999. Corrosion of stainless steel by gaseous I_2. J. Nucl. Mater. 265, 161–177.

Zoulalian, A., Belval-Haltier, E., 1998. Interaction between molecular iodine in gaseous phase and a coat of paint – influence of temperature, humidity, and hydrothermal treatment on iodine trapping kinetics. Nucl. Technol. 122, 196–210.

Zoulalian, A., Belval-Haltier, E., 2000. Interaction between molecular iodine in a gas phase and paints aged in a nuclear power plant. Nucl. Technol. 130, 362–371.